serval
serveur académique lausannois

UNIL | Université de Lausanne
Faculté de biologie
et de médecine

Astrocytes are key but indirect contributors to the development of the symptomatology and pathophysiology of Huntington's disease

Authors: Cécile Meunier[1], Nicolas Merienne[2,3], Charlotte Jollé[1], Nicole Déglon[2,3], Luc Pellerin[1]

Affiliations: [1]Department of Physiology, University of Lausanne, Switzerland; [2]Department of Clinical Neurosciences, Laboratory of Cellular and Molecular Neurotherapies (LCMN), Lausanne University Hospital, Lausanne, Switzerland; [3]Neuroscience Research Center (CRN), LCMN, Lausanne University Hospital, Lausanne, Switzerland

Running title: Astrocytes in Huntington's disease

Number of words:

Title	17
Abstract	214
Main points	33
Introduction	549
Materials and methods	356
Results	2571
Discussion	1474
Acknowledgement and Authors contributions	131
References	1171
Figure legends	1131
Total	**7798**

Number of Figures: 8

Number of Supplemental Figure: 5

Number of Supplemental Material: 1

Correspondence should be addressed to:

Prof. Luc Pellerin

Department of Physiology

7 Rue du Bugnon

1005 Lausanne

Switzerland

Email: Luc.Pellerin@unil.ch

Tel: +41 21 692 5547

Fax: +41 21 692 5505

2

Main points:

- **Astrocytes expressing mutant *Huntingtin* are key contributing actors to behavioural phenotype and cellular alterations**
- **Alterations of glial glutamate metabolism are caused by astrocyte-specific and**

5

- **neuron-specific expression of mutant *Huntingtin***

Key words:

Glia; Polyglutamine expansion; Adeno-associated viral vectors; Striatum; Mouse model

2

Abstract

Huntington's disease (HD) is a fatal neurodegenerative disease in which an early and selective vulnerability of striatal Spiny Projection Neurons is observed. However, several studies have

5   highlighted the implication of glial cells, and in particular astrocytes, in the pathophysiological mechanisms of this disease. A better understanding of the respective contributions of neurons and astrocytes in HD is needed and would be important for the development of new therapeutic approaches. Today, no comparable *in vivo* models expressing the mutant HTT selectively in astrocytes or in neurons are available. In this study, we developed comparable cell-type specific

10   mouse models expressing a fragment of *Huntingtin* specifically in neurons, astrocytes, or in both cell populations of the adult mouse basal ganglia circuit. These models allowed us to unravel some behavioural alterations occurring as soon as 4 weeks post-injection in the neuron-specific model, and additional dysfunctions when *mHTT* was co-expressed in astrocytes. We further evaluated the differential contribution of astrocytes compared to neurons in several

15   pathophysiological mechanisms such as mHTT protein aggregation, astrogliosis and neuronal dysfunction. We observed that transcriptional alterations within the glial glutamatergic clearing system were caused both by both astrocytic and neuronal expression of *mHTT*. We anticipate that our study will help to better understand the contributions of astrocytes to HD and guide future therapeutic efforts.

20

Introduction

Huntington's disease (HD) is a rare neurodegenerative disease affecting around 5-7 per 100.000 people worldwide. The pathology is caused by an autosomal dominant genetic mutation

5   located on the *IT15* gene (*Huntingtin* gene, *HTT*), coding for the Huntingtin protein (HTT; (The Huntington's Disease Collaborative Research Group 1993). CAG repeats within the Exon 1 ≥ 40 cause the formation of a toxic polyglutamine stretch at the N-terminal part of the protein. Patients develop progressive motor, cognitive, psychiatric and physiological alterations starting between age 35 and 50 leading to death within 15-20 years (Roos 2010). HD pathophysiology is marked

10   by an early degeneration of the Spiny Projection Neurons (SPNs) of the striatum, which represent more than 90% of the striatal neurons. The abnormal polyglutamine stretch on HTT leads to a toxic gain of function of the protein, resulting in a pathological accumulation of HTT aggregates with cellular and transcriptional alterations (Zuccato et al. 2010). Up to now, the vulnerability of SPNs is not completely understood. *HTT* is ubiquitously expressed in the brain

15   and in peripheral tissues, and differences in *HTT* expression levels are not sufficient to explain this preferential vulnerability (Fusco et al. 1999).

During the last decades, numerous studies demonstrated the essential role of astrocytes in key biological functions (Chung et al. 2015). Surprisingly, only few pathophysiological alterations linked to glial cells have been described in HD patients and animal models. A

20   progressive astrogliosis has been observed in the post-mortem brain of HD patients and animal models, together with alterations of the glutamate-glutamine cycle and of ascorbic acid metabolism (Acuna et al. 2013; Faideau et al. 2010). Mouse models expressing mutant *HTT* *(mHTT)* specifically in astrocytes have been previously developed to confirm the implication of these cells in HD (Bradford et al. 2009; Faideau et al. 2010). However, the small-transduced

25   area obtained with lentiviral vectors has limited the evaluation of the contribution of astrocytes to the behavioral phenotype. Importantly, the differences in terms of *HTT* constructions and CAG

repeats number make the comparison of transgenic models expressing *mHTT* in neurons or in astrocytes difficult.

Viral vectors such as Adeno-Associated Viruses (AAV) are potent tools to express a transgene in the central nervous system. The modulation of AAV capsids together with cell-type

5   specific promoters have opened the possibility to shift the expression of a transgene from one cell population to another (Merienne et al. 2013). Furthermore, AAV vectors have been already used to efficiently express *mHTT* in the mouse brain (Franich et al. 2008; Hult et al. 2011). In this study, we took advantage of AAV properties and specific promoters to develop mouse models in which *mHTT* is selectively expressed in neurons or in astrocytes of the basal ganglia

10   system, with a stable and similar expression rate. Additionally, we obtained a parallel expression of *mHTT* in both cell populations by co-injecting the two cell-type specific AAVs. With these models, we were able to evaluate behavioral, cellular and molecular dysfunctions as soon as 4 weeks post-injection. This study highlights the respective contributions and vulnerabilities of neurons and astrocytes in Huntington's disease, and an indirect but essential role of glial cells in

15   the pathophysiological mechanisms. It also opens the possibility to apply a similar approach to study the individual contribution of distinct cell types, including different glial cell types, in other neurodegenerative diseases.

Materials and methods

The complete Experimental Procedures section can be found as online Supplemental

20   Experimental Procedure.

Animals

All animal procedures were approved by the Swiss "Service de la Consommation et des Affaires Vétérinaires" (SCAV, authorization n°2747.0, see Supplemental Experimental Procedures).

Injections

All mice were injected at 11 weeks old. Injections parameters, doses and surgical procedures can be found in Supplemental Experimental Procedure.

Behavioral tests

Living conditions such as testing time, room and light were kept identical between groups. Order of mice was balanced between HTT171-82Q and HTT171-18Q groups. Investigator was the same for all tests and between all groups, and behavioral tests started one week before euthanasia (see Supplemental Experimental Procedure).

Brain samples processing

After lethal injection of Pentobarbital solution (150mg/kg), mice were either quickly decapitated to further extract mRNA and proteins of striatal eGFP-positive punches with TRIzol Reagent ® (see Suplemental Experimental Procedures), or fixed by intra-cardiac perfusion of Sodium-Phosphate buffer (0.4M) with Paraformaldehyde 4% for immunohistochemical analysis (see Supplemental Experimental Procedure).

Immunohistochemistry

$20\mu m$ free-floating coronal brain sections were used in this study. Primary and secondary antibodies are described in Supplemental Experimental Procedures. For image acquisition, except when mentioned in figure legend, identical parameters were maintained between all groups, and quantification analyses were performed on raw, unmodified pictures. ImageJ 1.44p software was used for all analyses (See Supplemental Experimental Procedure).

RT-qPCR

After mRNA extraction, DNAse treatment and random-primed first strand complementary DNA (cDNA) synthesis were performed on samples (see Supplemental Experimental Procedures). Real-Time quantitative PCR was performed with StepOne Real Time PCR System

(ThermoFisher Scientific). Detailed primer sequences and protocols are available in Supplemental Experimental Procedures.

Western blot

After protein extraction, proteins from each sample were loaded on polyacrylamide gel for further immunoblot analysis (see Supplemental Experimental Procedures). Groups were equally represented on each membrane to allow further comparisons. Details about antibodies and analysis are described in Supplemental Experimental Procedures.

Statistical analysis

Data were analyzed using Statistica 10 Statsoft software. Student's t test, Factorial ANOVA or Repeated-measures ANOVA were performed, followed by post hoc LSD Fisher analysis. P value <0.05 was considered as significant. Data are expressed as mean ± SEM (see Supplemental Experimental Procedure).

Results

AAV2/5 with distinct promoters leads to cell-type specific expression of *mHTT* in the adult mouse striatum

In order to obtain cell-type specific transgene expression in the mouse striatum, Adeno-Associated Viral vectors 2/5 (AAV2/5) containing either the Chicken-β Actin promoter (CBA) or a truncated form of the Glial Fibrillary Acidic Protein promoter including three enhancers (de Leeuw et al. 2006) were developed. AAV2/5 expressing the enhanced green fluorescent protein (eGFP) under the CBA or Gfa2(B)3 promoter (CBA-eGFP or Gfa2(B)3-eGFP) was injected in the striatum of adult mice to evaluate their respective tropism (Figure 1A). Confocal microscopy analysis revealed that more than 90% of cells transduced with CBA-eGFP were NeuN-positive, whereas more than 90% of cells transduced with Gfa2(B)3-eGFP were positive for Glutamine Synthetase (GS, Figure 1B), confirming a specific transduction of neurons or astrocytes,

7

respectively. Furthermore, we qualitatively observed that the AAV2/5 transduces a large area of the mouse striatum, both in the antero-posterior and medio-lateral axes (Supplemental Figure S1A). We evaluated the ability of AAVs vectors to transduce other structures of the basal ganglia circuit by co-injecting an AAV2/5 expressing mCherry under the CBA promoter and an AAV2/5

5   expressing eGFP under the Gfa2(B)3 promoter in the striatum. Both eGFP- and mCherry-positives cells were detected in the pallidum, nucleus accumbens, substantia nigra and in the primary motor cortex (Supplemental Figure S1B). In summary, the two AAV2/5 viral vectors differing only by their respective promoter represent efficient tools to specifically express a transgene in neurons or in astrocytes, in the adult mouse striatum and in part of the basal

10   ganglia circuit.

The cell-type specific expression of mHTT was next obtained by cloning a sequence coding for the first 171 amino acids of the human HTT protein under the control of either the CBA or Gfa2(B)3 promoter. The *mHTT* contained 82 CAG repeats (HTT171-82Q), whereas the control *HTT* contained only 18 CAG repeats (HTT171-18Q-HA, (de Almeida et al. 2002). AAV2/5

15   viral vectors expressing the mutant or the control *HTT* under the CBA or the Gfa2(B)3 promoter were injected in the striatum at low dose ($5E10^7$ viral genome/site), thus allowing a specific expression of control or mutant *HTT* in neurons or in astrocytes and a progressive appearance of the pathology (CBA-HTT171-82Q, CBA-HTT171-18Q, Gfa2(B)3-HTT171-82Q or Gfa2(B)3-HTT171-18Q mice, Figure 1C). Additionally, to obtain *HTT* expression in both cell populations at

20   once, co-injection of neuron-specific and astrocyte-specific viral vectors was performed (CBA/Gfa2(B)3-HTT171-82Q or CBA/Gfa2(B)3-HTT171-18Q mice, $5E10^7$ viral genome/site per viral vector, Figure 1C). Visualization of the transduced area and validation of the injection accuracy were performed by co-injecting in each mouse either the CBA-eGFP or the Gfa2(B)3-eGFP viral vector at very low dose ($4E10^6$ viral genome/site). Reverse-Transcription Quantitative

25   Polymerase Chain Reaction (RT-qPCR) with primers recognizing both the murine and human

8

HTT mRNA confirmed *mHTT* expression levels approximately 13 fold higher than the endogenous *Htt* level in non-injected mice for the neuronal and the astrocytic model from 4 to 16 wpi (Figure 1D). The co-injection of both CBA-HTT171-82Q and Gfa2(B)3-HTT171-82Q AAV2/5 led to an expression level of *mHTT* approximatively 42 fold higher than the level of endogenous

5 *Htt* from 4 to 16 wpi. A statistical analysis confirmed a similar expression between the neuronal and the astrocytic model, a significant increase in CBA/Gfa2(B)3-HTT171-82Q mice (double model) and a stable expression of the transgene from 4 to 16 wpi in each group. Altogether, optimization of promoters and injection parameters with AAV2/5 enable a high, stable and similar expression of *mHTT* between neurons and astrocytes *in vivo*.

10 Co-expression of *mHTT* in neurons and in astrocytes does not exacerbate behavioral deficits induced by neuronal *mHTT* but caused additional alterations.

HD patients develop motor, psychiatric, and cognitive symptoms. Thus, the phenotype of the three mouse models was characterized by measuring anxiety, spontaneous motor activity, locomotor coordination and the presence of abnormal movements.

15 Thigmotaxic behavior during an Open Field task corresponds to the tendency of a mouse to travel closer to the walls and less in the arena center, which is a recognized marker of anxiety in HD mouse models (Pla et al. 2014). Here, mice expressing *mHTT* specifically in neurons or in both neurons and astrocytes travel significantly more in the external field compared to control mice, from 4wpi to 12 wpi (Figure 2A). This suggests an increased anxiety in these two models.

20 No significant thigmotaxic behavior was observed in mice expressing *mHTT* only in astrocytes. Analysis of the total distance traveled in the Open Field did not reveal spontaneous motor activity alterations in mice expressing *mHTT* only in neurons or in astrocytes, but a significant hyperactivity appeared from 12 wpi to 16 wpi in the group with *mHTT* co-expressed in both cell types (Figure 2B).

9

Locomotor coordination in a forced motor task was evaluated with the Rotarod Accelerated Test. The expression of *mHTT* only in neurons induced a significant deficit in locomotor coordination at 12 wpi and 16 wpi, and a deficit at 8 and 16 wpi when *mHTT* is expressed in both cell types (Figure 2C). In contrast, *mHTT* expression restricted to astrocytes

5 only led to a mild locomotor alteration in this test at 16 wpi (Figure 2C). Then abnormal movements such as clasping were evaluated in each mouse model. Only the co-expression of *mHTT* in both neurons and astrocytes was able to significantly induce the appearance of clasping behavior starting at 8 wpi (Figure 2D). Finally, physiological alterations such as weight loss have also been described in HD patients (van der Burg et al. 2009). However, whether

10 these alterations are the consequence of *mHTT* expression in the brain or in peripheral organs is still unclear. Here, the weight gain in each model following the surgery up to euthanasia was determined. A significant decrease in weight gain was observed in mice expressing *mHTT* only in neurons at 16 wpi and in mice expressing *mHTT* in neurons and in astrocytes at the same time, but not when the expression was restricted to astrocytes (Figure 2E).

15 Altogether, these results demonstrate that expression of *mHTT* restricted to neurons of the basal ganglia circuit is sufficient to induce significant behavioral and physiological alterations, whereas its expression only in astrocytes only induces mild locomotor deficits.. Furthermore, the co-expression of *mHTT* both in neurons and in astrocytes did not exacerbate deficits observed in the neuron-specific model but additionally induced hyperactivity and

20 clasping.

<u>Striatal neurons and astrocytes exhibit distinct mHTT aggregation patterns</u>

Considering the different behavioral phenotypes observed between the three mouse models, the histopathological consequences of *mHTT* expression in striatal cells was investigated. Specific immunolabelings for aggregated mHTT revealed the aggregation of the

25 protein in the three mouse models as soon as 4 wpi (Figure 3A), whereas no detectable mHTT

aggregates were observed in any of the control groups (Supplemental Figure S2A). No sign of aggregates spreading from one cell population to another was observed in the two cell-type specific models (Supplemental Figure S2B). Consistent with the presence of eGFP- or mCherry-positive cells in other structures, mHTT aggregates were observed in the lateral globus pallidus,

5 the nucleus accumbens and the cortex, in both CBA-HTT171-82Q and Gfa2(B)3-HTT171-82Q mice (Supplemental Figure S3A). mHTT aggregates were also observed in the substantia nigra pars compacta, except in the astrocytic model. No aggregates were observed in the arcuate nucleus of the hypothalamus (Supplemental Figure S3B).

Interestingly, quantifications confirmed the presence of a higher number of aggregates at

10 16 wpi when mHTT was expressed in neurons compared to astrocytes (Figure 3B). The co-expression of *mHTT* in neurons and in astrocytes led to a higher number of aggregates compared to the two cell-type specific models at 16 wpi (Figure 3B). A previous study distinguished large mHTT aggregates with a diameter >3μm and small HTT inclusions with a diameter <3μm (Sahl et al. 2012). Using this criteria, quantifications indicated a higher proportion

15 of large aggregates in neurons compared to small aggregates, whereas the opposite pattern was observed in astrocytes (Figure 3C). Furthermore, high magnification confocal imaging revealed large aggregates in nuclear or cytoplasmic compartments whereas small aggregates could be located in nuclear, cytoplasmic or dendritic/process compartments (Figure 3D). Considering these results, it became clear that mHTT in striatal neurons and in astrocytes

20 undergoes aggregation or clearing processes specific for each cell population.

mHTT expression in astrocytes exacerbates early dysfunction of striatal SPNs

Dysfunction of the striatal SPNs is closely linked to the phenotype of HD mouse models and to deficits observed in HD patients (Guo et al. 2012). Here, the protein and mRNA levels of Dopamine- and cAMP-Regulated PhosphoProtein, 32kDa (DARPP-32, *Ppp1r1b*), a typical

25 marker of functional SPNs, were determined. An histological analysis revealed a decrease of

DARPP-32 staining intensity in the striatum of CBA-HTT171-82Q mice, starting at 8 wpi, whereas no DARPP-32 lesion was observed in Gfa2(B)3-HTT171-82Q mice, compared to control mice (Figure 4A-B). The DARPP-32 lesion was exacerbated when *mHTT* was co-expressed in both cell populations, and detectable as early as 4 wpi (Figure 4A-B). These results

5 were confirmed at the mRNA level by RT-qPCR, showing a significant decrease (53.8%) of *Ppp1r1b* expression in CBA-HTT171-82Q mice from 8 wpi to 16 wpi (Figure 4C). The co-expression of *mHTT* both in neurons and astrocytes exacerbated this dysfunction by inducing a 66.4% decrease of *Ppp1r1b* expression from 4 wpi to 16 wpi. We confirmed the absence of neuronal death in all groups by NeuN immunolabeling (Supplemental Figure S4).

10 Here, intrinsic neuronal alterations caused by mHTT appears to be sufficient to trigger early dysfunction of SPNs in HD. However, even if *mHTT* expression restricted to astrocytes is not sufficient to induce alterations in non-transduced SPNs, astrocytes expressing *mHTT* contribute to accelerate the pathology.

Co-expression of *mHTT* in neurons and astrocytes induces early signs of astrogliosis

15 A progressive astrogliosis was previously described in HD patients and in animal models (Faideau et al. 2010). The origin and contribution of this pathophysiological mechanism to the development of the disease are still poorly described. In this context, it was interesting to determine if the neuronal expression of *mHTT* was sufficient to trigger astrocytic modifications such as astrogliosis.

20 A first analysis of total *Gfap* mRNA levels shown no difference between groups expressing *mHTT* and control groups in the three different mouse models (Figure 5A). In a second step, Gfap protein level was evaluated using immunohistochemistry by measuring the integrated density of labeling in striatal Gfap-positive astrocytes. A significant increase in was observed at 16 wpi when *mHTT* was co-expressed in both neurons and astrocytes, but not when

12

mHTT was only expressed in neurons or in astrocytes (Figure 5B). Furthermore, the evaluation of a putative hypertrophic morphology of striatal astrocytes indicated an increase total Gfap-positive area only in mice expressing *mHTT* in both neurons and astrocytes (Figure 5C-D). Interestingly, these results can not be explained by the total number of Gfap-positive cells

5   (Supplementary Figure 5B). In addition, no difference was observed at 4wpi between the three models as well as between mutant and control groups, indicating that this result was not a mere consequence of the injection (Supplementary Figure 5A). Our data suggest that at these stages *mHTT* only in astrocytes is not sufficient to trigger astrogliosis, and that a concomitant neuronal dysfunction seems to be required to observe a glial reactivity.

10   <u>Transcriptional alterations of the glutamate-glutamine cycle in HD are caused by both neuronal and astrocytic *mHTT* expression</u>

In HD, glutamatergic excitotoxicity is a major contributor of neuronal degeneration (Estrada Sanchez et al. 2008). Glutamate-induced toxicity can be caused by a dysfunction of glutamate clearing by astrocytes and by alterations of neuronal N-methyl-D-Aspartate receptors

15   (NMDAR), including transcriptional dysfunctions (Zuccato et al. 2010).

An analysis of the glutamate recycling process in the three mouse models was carried out by evaluating mRNA levels of the two glutamate transporters Excitatory Amino Acid Transporters 1 and 2 (Glast, *Slc1a3* and Glt1, *Slc1a2*). In addition, mRNA levels of the α_2 subunit of the Na^+/K^+-ATPase (*Atp1a2*), which is a crucial actor in ion exchanges needed for the

20   maintenance of glutamate transporter activity, were determined, together with Glutamine Synthetase (Gs, *Glul*), which is the key enzyme for the astrocytic glutamate conversion to glutamine. RT-qPCR showed that the expression of *mHTT* in astrocytes leads to a significant decrease of *Slc1a2* (Glt1) and *Slc1a3* (Glast) mRNA levels, starting at 12 wpi and 8 wpi respectively (Figure 6A-B). In this model, *Atp1a2* and *Glul* (Gs) mRNA significantly decreased at

25   12 and 4 wpi respectively (Figure 6C-D). Interestingly, *mHTT* in neurons also led to a significant decrease of these four components of the astrocytic glutamate clearing process (Figure 6A-D).

Finally, the co-expression of *mHTT* in the two cell populations strongly exacerbated these transcriptional alterations for *Slc1a2*, *Slc1a3*, *Atp1a2* and Glul (Figure 6A-D). Western blot analysis confirmed a significant decrease of Glt1 protein levels only in but the double model (Figure 6E).

In parallel, mRNA levels of two major subunits of the NMDA receptor (NMDAR) were analyzed: NR1 (*Grin1*) which is not mainly affected by *mHTT*, and Nr2b (*Grin2b*) which is highly associated with glutamatergic excitotoxicity (Ali and Levine 2006). Results showed no alteration of *Grin1* expression levels in any of the three models, except for a mild but significant decrease at 12 wpi in CBA-HTT171-82Q mice (Figure 6F). On the other hand, the neuron-specific expression of *mHTT* was sufficient to induce a significant decrease of *Grin2b* mRNA levels at 8, 12 and 16 wpi, whereas this decrease was not significant when *mHTT* was expressed in both neurons and in astrocytes, except at 16 wpi (Figure 6G). No such alteration was found in the astrocyte-specific mouse model (Figure 6G). In summary, it was found that both neuron- and astrocyte-specific *mHTT* expression lead to alteration of various astrocytic components of the glutamate recycling process at the transcriptional level. In contrast, only *mHTT* expressed in neurons is able to alter the expression of the Nr2b subunit.

DARPP-32 and key elements of the Glutamate-glutamine cycle are closely linked to locomotor performances

In this study several pathophysiological hallmarks of HD and their evolution in three distinct models have been described. In order to analyze a putative link between transcriptional deficits and behavioral alterations, we performed Pearson correlation analysis on the expression levels of key elements involved in HD pathophysiology (*Ppp1rb, Gfap*) as well as in the Glutamate-Glutamine cycle (*Slc1a2, Slc1a3, Atp1a2, Glul, Grin1, Grin2b*), and on behavioral performances of mice. This analysis was ran on all time points, both in HTT171-18Q and HTT171-82Q mice, separately in the three models. A *p value* reflecting the probability of true correlation was

14

calculated for each Pearson correlation and corrected for multiple testing according to the

Benjamini and Hochberg method (Benjamini and Hochberg 1995).

This analysis showed distinct correlation patterns between each model. In CBA-HTT171

mice, we showed significant positive correlations between genes involved in the Glutamate-

5   Glutamine cycle (Glt1, Glast, Atp1a2, GS, Figure 7A). Interestingly, this cluster also includes

DARPP-32, which positively correlates with all these genes and in particular Glt1 (r = 0.93,

FDR<0.0001). In the astrocytic model, we only observed positive correlations between the

Glutamate-Glutamine cycle elements but not with DARPP-32, except for Glt1 (Figure 7B).

Finally, in mice expressing *mHTT* in neurons and in astrocytes, the cluster which brings together

10   Glutamate-Glutamine cycle genes and DARPP-32 is present (Figure 7C). Interestingly, in this

more severe pathological context, significant positive correlations are observed between

behavioral performances, mRNA levels of DARPP-32 and elements of the Glutamate-Glutamine

cycle (Figure 7C). These results suggest an important link between expression levels of DARPP-

32 and glutamate recycling, in particular Glt1, that are also related to behavioral performance

15   such as motor coordination, locomotion and abnormal clasping.

Discussion

In this study, we developed three cell-type specific mouse models of HD in order to analyze

the respective contributions of neurons and astrocytes to the pathophysiology of the disease.

20   AAV2/5 expressing *mHTT* under CBA or Gfa2(B)3 promoters allowed us to obtain high, stable

and similar expression levels of *mHTT* in neurons and in astrocytes of part of the basal ganglia

circuit, and to co-express *mHTT* in both cell populations. All models exhibited typical behavioral,

cellular and molecular dysfunctions of HD, but their evolution and severity differed (Figure 8A-C).

Expression of mHTT in basal ganglia neurons is sufficient to affect body weight

The significant decreased weight gain observed at 16 wpi in models expressing *mHTT* in neurons or in both neurons and astrocytes was an unexpected result. A progressive body weight loss is observed in the late stages in HD patients, but only reproduced in transgenic mouse models with ubiquitous expression of a short *HTT* fragment (Phan et al. 2009). In contrast,

5   transgenic mice expressing full-length *HTT* demonstrate increased body weight (Van Raamsdonk et al. 2006). Interestingly, the specific expression of a long or a short fragment of *mHTT* in the hypothalamus induced increased body weight in mice (Hult et al. 2011). These studies highlighted the role of hypothalamic dysfunctions in metabolic alterations observed in some mouse models, but also suggested that the body weight loss observed in patients at late

10   stages of the disease and in short fragment mouse models would be mainly due to *mHTT* effects on peripheral organs and tissues (Carroll et al. 2015).

In our study we showed that the expression of a short fragment in part of the basal ganglia circuit is sufficient to explain at least part of the metabolic dysfunction linked to body weight loss. Importantly, AAV2/5 used in this study transduced the nucleus accumbens (NAcc), in which we

15   observed mHTT-positive aggregates. The NAcc and the striatum are key components of the meso-limbic dopaminergic system that directly interact with the ventral tegmental area and the lateral hypothalamus to regulate the motivational and rewarding aspects of food intake (Wise 2006). In this context, dysfunctional SPNs could potentially alter the balance between the hypothalamus and the rewarding system. In future studies, it would be interesting to investigate

20   the effect of *mHTT* in the hypothalamus or in the basal ganglia circuit specifically on food intake regulation.

Distinct mHTT aggregation and/or clearing processes are observed in neurons and astrocytes

An early aggregation of mHTT is observed in the three mouse models as soon as 4 wpi, which is characteristic of models expressing short *mHTT* fragment (de Almeida et al. 2002).

25   Additionally, we observed fewer numbers of aggregates in astrocytes compared to neurons, and

16

the majority of detected aggregates in astrocytes had a diameter < 3 μm. This suggests that glial

cells possess distinct mechanisms of cleavage and/or clearing of mHTT compared to neurons.

We expressed only the first 171 amino acids of HTT, excluding most putative cleavage sites by

caspases or calpains located after the first 200 amino acids (Zuccato et al. 2010). However, a

5   previous study described a Cp-2 cleavage site for cysteine proteases, located at the position

Arg[167] and acting both on mHTT toxicity and on the aggregation process (Ratovitski et al. 2009).

One plausible hypothesis is that cell-type specific expression or regulation of cysteine proteases

between neurons and astrocytes could explain the differential aggregation processes.

Clearing of mHTT aggregates in the nucleus and in the cytoplasm depends on the Ubiquitin-

10   Proteasome system, which was shown to have a higher activity in glial cells compared to

neurons, leading to higher efficiency for the degradation of misfolded protein (Tydlacka et al.

2008). Previous studies demonstrated that an increased proteasome activity could lead to a

higher number of small inclusions compared to diffuse forms (Venkatraman et al. 2004), which is

consistent with the pattern observed here in astrocytes. Small HTT inclusions were also

15   associated with a higher toxicity, whereas large inclusions or diffuse aggregates could be linked

to a protective mechanism by the cell (Arrasate et al. 2004). Neurons being the most affected by

mHTT, it may appear contradictory that astrocytes present mainly the most toxic form of mHTT

aggregates and neuronal cells the most protective one. Neuronal cells having a lower

proteasome activity, they could potentially compensate the higher total number of aggregated

20   mHTT by a protective mechanism leading to the formation of large and diffuse aggregates

concomitantly with small inclusions. In contrast, a higher proteasomal activity combined with

specific cleavage mechanisms in astrocytes could explain a fewer total number of aggregates

with a higher proportion of small inclusions that could not be degraded by the proteasome.

mHTT in neurons affects mRNA levels of key elements of the glial glutamate-glutamine cycle

Despite the smaller number of mHTT aggregates observed in astrocytes, we found that glial cells are affected at the transcriptional level with a significant decrease of GLT1, GLAST, GS and Na^+/K^+-ATPase $\alpha2$ subunit mRNA levels. These results are highly consistent with previous studies on HD patients and animal models (Estrada Sanchez et al. 2008). Furthermore, no

5   behavioral or neuronal alterations were induced by *mHTT* in astrocytes, suggesting an ability of glial cells to compensate at least partially these down-regulations to maintain a sufficient glutamatergic recycling activity for surrounding cells to prevent neuronal dysfunction.

We observed a decreased mRNA expression of the two main glutamate transporters GLT1 and GLAST, as well as of glutamine synthetase and the α_2 subunit of the Na^+/K^+-ATPase when

10   mHTT was expressed only in neurons. In a previous study, neuron-specific expression of *mHTT* by injection of a lentiviral vector did not lead to a decrease of GLT1 or GLAST expression at the protein level, which is coherent with our present results. However the mRNA levels of these two transporters were not investigated (Faideau et al. 2010). Glt1, Glast, Gs or Atp1a2 being mainly expressed by astrocytes, our results suggest that a neuronal dysfunction could indirectly affect

15   astrocytic glutamate recycling components at the transcriptional level in a positive or negative manner. *In vitro* experiments on primary cultures of astrocytes suggested that soluble factors could be released by neurons and act via a *kappa* B-motif binding protein (KBBP) to increase GLT1 mRNA levels (Yang et al., 2009). Other studies highlighted the role of endothelins as regulators of GLT1 expression and activity, especially in a pathological context (Glisic et al.,

20   2012).. To our knowledge, an indirect contribution of *mHTT* in neurons to transcriptional alterations of glutamate recycling components in astrocytes was not shown in previous studies, and which pathways and factors are involved in this mechanism remain to be determined.

Relationship between locomotor activity, DARPP-32 expression and glutamate clearing

Interestingly, in the double model we observed a significant correlation between DARPP-32

25   mRNA and behavioral deficits in locomotor coordination, spontaneous motor activity and

18

clasping. Furthermore, correlation analysis also showed a significant link between DARPP-32 and Glt1 mRNA levels. In the striatum, the DARPP-32 protein acts as a pivotal element to modulate activity and responses of SPNs as a consequence of multiple signal integration (Greengard et al. 1999). DARPP-32 phosphorylation and activity are mainly regulated by

5   dopaminergic inputs, but are also linked to glutamatergic neurotransmission (Blank et al. 1997). However, to our knowledge, a link between DARPP-32 and glutamate clearing by astrocytes at the mRNA level has never been shown. Future studies aiming at understanding how expression of DARPP-32 and astrocytic glutamate transporters such as Glt1 are concomitantly modulated will bring important new insights in the regulation of glutamatergic inputs on SPNs.

10   *Perspectives*

Currently, no treatment is available for HD patients. Several therapeutic strategies are considered, such as pharmacological approaches or gene therapy (Glorioso et al. 2015; Venuto et al. 2012). For gene therapy in neurodegenerative diseases, the question of targeting only neurons or additionally surrounding astrocytes still remains (Furman et al. 2012). Several

15   approaches are available to directly target mHTT expression at the RNA level (small-hairpin RNA, shRNA) or at the DNA level (Clustered Regularly Interspaced Short Palindromic Repeats, CRISPR system; (Moore et al. 2010; Wright et al. 2016), and viral vectors were recently designed to express shRNA specifically in astrocytes (Merienne et al. 2015). These approaches will be important in the future to determine the necessity to treat both neurons and astrocytes in

20   HD. Finally, recent major technological advances for single cell profiling were made (Heiman et al. 2008; Zhang et al. 2014). Their combination with cell-type specific expression of pathological transgenes will also be essential to precisely dissect the respective contribution of each brain cell population to neurodegenerative diseases, and to efficiently target key mechanisms acting on the whole cellular environment. Considering the high flexibility of viral vector approaches, we

25   believe that the present study not only provides some interesting insights about the contribution

of astrocytes to the pathophysiology of HD, but also reveals the potential of such an approach

for applications in the broader context of neurodegenerative diseases.

Author contributions:

C.M, N.M and L.P designed the study. C.M, N.M and N.D designed the plasmids and the production of viral vectors. C.M performed the behavioral tests. C.M and C.J performed post-

5 mortem analyses. C.M and N.M performed microscopic imaging. C.M and L.P wrote the manuscript. C.M, N.M, C.J, N.D and L.P corrected the manuscript.

Acknowledgments:

References:

Acuna AI, Esparza M, Kramm C, Beltran FA, Parra AV, Cepeda C, Toro CA, Vidal RL, Hetz C, Concha, II and others. 2013. A failure in energy metabolism and antioxidant uptake precede symptoms of Huntington's disease in mice. Nat Commun 4:2917.

Ali NJ, Levine MS. 2006. Changes in expression of N-methyl-D-aspartate receptor subunits occur early in the R6/2 mouse model of Huntington's disease. Dev Neurosci 28:230-8.

Arrasate M, Mitra S, Schweitzer ES, Segal MR, Finkbeiner S. 2004. Inclusion body formation reduces levels of mutant huntingtin and the risk of neuronal death. Nature 431:805-10.

Benjamini Y, Hochberg Y. 1995. Controlling the False Discovery Rate: A Practical and Powerful Approach to Multiple Testing. Journal of the Royal Statistical Society 57:289.

Blank T, Nijholt I, Teichert U, Kugler H, Behrsing H, Fienberg A, Greengard P, Spiess J. 1997. The phosphoprotein DARPP-32 mediates cAMP-dependent potentiation of striatal N-methyl-D-aspartate responses. Proc Natl Acad Sci U S A 94:14859-64.

Bradford J, Shin JY, Roberts M, Wang CE, Li XJ, Li S. 2009. Expression of mutant huntingtin in mouse brain astrocytes causes age-dependent neurological symptoms. Proc Natl Acad Sci U S A 106:22480-5.

Carroll JB, Bates GP, Steffan J, Saft C, Tabrizi SJ. 2015. Treating the whole body in Huntington's disease. Lancet Neurol 14:1135-42.

Chung WS, Welsh CA, Barres BA, Stevens B. 2015. Do glia drive synaptic and cognitive impairment in disease? Nat Neurosci 18:1539-45.

de Almeida LP, Ross CA, Zala D, Aebischer P, Deglon N. 2002. Lentiviral-mediated delivery of mutant huntingtin in the striatum of rats induces a selective neuropathology modulated by polyglutamine repeat size, huntingtin expression levels, and protein length. J Neurosci 22:3473-83.

de Leeuw B, Su M, ter Horst M, Iwata S, Rodijk M, Hoeben RC, Messing A, Smitt PS, Brenner M. 2006. Increased glia-specific transgene expression with glial fibrillary acidic protein promoters containing multiple enhancer elements. J Neurosci Res 83:744-53.

Estrada Sanchez AM, Mejia-Toiber J, Massieu L. 2008. Excitotoxic neuronal death and the pathogenesis of Huntington's disease. Arch Med Res 39:265-76.

Faideau M, Kim J, Cormier K, Gilmore R, Welch M, Auregan G, Dufour N, Guillermier M, Brouillet E, Hantraye P and others. 2010. In vivo expression of polyglutamine-expanded huntingtin by mouse striatal astrocytes impairs glutamate transport: a correlation with Huntington's disease subjects. Hum Mol Genet 19:3053-67.

Franich NR, Fitzsimons HL, Fong DM, Klugmann M, During MJ, Young D. 2008. AAV vector-mediated RNAi of mutant huntingtin expression is neuroprotective in a novel genetic rat model of Huntington's disease. Mol Ther 16:947-56.

Furman JL, Sama DM, Gant JC, Beckett TL, Murphy MP, Bachstetter AD, Van Eldik LJ, Norris CM. 2012. Targeting astrocytes ameliorates neurologic changes in a mouse model of Alzheimer's disease. J Neurosci 32:16129-40.

Fusco F, Chen Q, Lamoreaux W, Figueredo-Cardenas G, Jiao Y, Coffman J, Surmeier DJ, Honig MG, Carlock LR, Reiner A. 1999. Cellular Localization of Huntingtin in Striatal and Cortical Neurons in Rats: Lack of Correlation with Neuronal Vulnerability in Huntington's Disease. Journal of Neuroscience 19:1189-1202.

Glisic D, Lehmann C, Figiel M, Odemis V, Lindner R, Engele J. 2012. A novel cross-talk between endothelin and ErbB receptors controlling glutamate transporter expression in astrocytes. J Neurochem 122:844-55.

Glorioso JC, Cohen JB, Carlisle DL, Munoz-Sanjuan I, Friedlander RM. 2015. Moving toward a gene therapy for Huntington's disease. Gene Ther 22:931-3.

Greengard P, Allen PB, Nairn AC. 1999. Beyond the Dopamine Receptor: the DARPP-32/Protein Phosphatase-1 Cascade. Neuron 23:435-447.

Guo Z, Rudow G, Pletnikova O, Codispoti KE, Orr BA, Crain BJ, Duan W, Margolis RL, Rosenblatt A, Ross CA and others. 2012. Striatal neuronal loss correlates with clinical motor impairment in Huntington's disease. Mov Disord 27:1379-86.

Heiman M, Schaefer A, Gong S, Peterson JD, Day M, Ramsey KE, Suarez-Farinas M, Schwarz C, Stephan DA, Surmeier DJ and others. 2008. A translational profiling approach for the molecular characterization of CNS cell types. Cell 135:738-48.

Hult S, Soylu R, Bjorklund T, Belgardt BF, Mauer J, Bruning JC, Kirik D, Petersen A. 2011. Mutant huntingtin causes metabolic imbalance by disruption of hypothalamic neurocircuits. Cell Metab 13:428-39.

Merienne N, Delzor A, Viret A, Dufour N, Rey M, Hantraye P, Deglon N. 2015. Gene transfer engineering for astrocyte-specific silencing in the CNS. Gene Ther 22:830-9.

Merienne N, Le Douce J, Faivre E, Deglon N, Bonvento G. 2013. Efficient gene delivery and selective transduction of astrocytes in the mammalian brain using viral vectors. Front Cell Neurosci 7:106.

Moore CB, Guthrie EH, Huang MT, Taxman DJ. 2010. Short hairpin RNA (shRNA): design, delivery, and assessment of gene knockdown. Methods Mol Biol 629:141-58.

Phan J, Hickey MA, Zhang P, Chesselet MF, Reue K. 2009. Adipose tissue dysfunction tracks disease progression in two Huntington's disease mouse models. Hum Mol Genet 18:1006-16.

Pla P, Orvoen S, Saudou F, David DJ, Humbert S. 2014. Mood disorders in Huntington's disease: from behavior to cellular and molecular mechanisms. Front Behav Neurosci 8:135.

Ratovitski T, Gucek M, Jiang H, Chighladze E, Waldron E, D'Ambola J, Hou Z, Liang Y, Poirier MA, Hirschhorn RR and others. 2009. Mutant huntingtin N-terminal fragments of specific size mediate aggregation and toxicity in neuronal cells. J Biol Chem 284:10855-67.

Roos RA. 2010. Huntington's disease: a clinical review. Orphanet J Rare Dis 5:40.

Sahl SJ, Weiss LE, Duim WC, Frydman J, Moerner WE. 2012. Cellular inclusion bodies of mutant huntingtin exon 1 obscure small fibrillar aggregate species. Sci Rep 2:895.

The Huntington's Disease Collaborative Research Group. 1993. A Novel Gene containing a Trinucleotide Repeat That is Expanded and Unstable on Hutnington's Disease Chromosomes. Cell 72:971-983.

Tydlacka S, Wang CE, Wang X, Li S, Li XJ. 2008. Differential activities of the ubiquitin-proteasome system in neurons versus glia may account for the preferential accumulation of misfolded proteins in neurons. J Neurosci 28:13285-95.

van der Burg JM, Bjorkqvist M, Brundin P. 2009. Beyond the brain: widespread pathology in Huntington's disease. Lancet Neurol 8:765-74.

Van Raamsdonk JM, Gibson WT, Pearson J, Murphy Z, Lu G, Leavitt BR, Hayden MR. 2006. Body weight is modulated by levels of full-length huntingtin. Hum Mol Genet 15:1513-23.

Venkatraman P, Wetzel R, Tanaka M, Nukina N, Goldberg AL. 2004. Eukaryotic proteasomes cannot digest polyglutamine sequences and release them during degradation of polyglutamine-containing proteins. Mol Cell 14:95-104.

Venuto CS, McGarry A, Ma Q, Kieburtz K. 2012. Pharmacologic approaches to the treatment of Huntington's disease. Mov Disord 27:31-41.

Wise RA. 2006. Role of brain dopamine in food reward and reinforcement. Philos Trans R Soc Lond B Biol Sci 361:1149-58.

Wright AV, Nunez JK, Doudna JA. 2016. Biology and Applications of CRISPR Systems: Harnessing Nature's Toolbox for Genome Engineering. Cell 164:29-44.

Yang Y, Gozen O, Watkins A, Lorenzini I, Lepore A, Gao Y, Vidensky S, Brennan J, Poulsen D, Won Park J and others. 2009. Presynaptic regulation of astroglial excitatory neurotransmitter transporter GLT1. Neuron 61:880-94.

Zhang Y, Chen K, Sloan SA, Bennett ML, Scholze AR, O'Keeffe S, Phatnani HP, Guarnieri P, Caneda C, Ruderisch N and others. 2014. An RNA-sequencing transcriptome and splicing database of glia, neurons, and vascular cells of the cerebral cortex. J Neurosci 34:11929-47.

Zuccato C, Valenza M, Cattaneo E. 2010. Molecular Mechanisms and Potential Therapeutical Targets in Huntington's Disease. Physiological Review 90:905-981.

5

10

Figure legends

Figure 1: Characterization of human *HTT* expression induced by cell-type specific AAV2/5

(A) Representative confocal pictures of mouse striatum 3 weeks post injection of CBA-eGFP
5 (upper panels) or Gfa2(B)3-eGFP AAV2/5 (lower panels). In CBA-eGFP mice, co-immunolabeling with a neuronal marker (NeuN, Neuronal nuclei) was performed, whereas in Gfa2(B)3-eGFP a co-immunolabeling with Glutamine Synthetase (GS), a marker of astrocytes, was performed. Scale bar = 20μm.

(B) Quantifications of the percentage of eGFP-positives cells that co-localized with NeuN or with
10 GS, three weeks after injection of CBA-eGFP or Gfa2(B)3-eGFP AAV2/5 in mouse striatum. Data are presented as mean ± SEM, quantifications were performed on 4-6 pictures/section, 4 sections/n, n= 4.

 (C) AAV2/5 vectors allowed expression of either control HTT171-18Q-HA (blue cells) or mutant HTT171-82Q (red cells), in neurons (CBA), in astrocytes (Gfa2(B)3), or in both neurons and
15 astrocytes (CBA/Gfa2(B)3), depending on the promoter. Forty mice/group were used in each experimental condition.. WPRE = Woodchuck Post-Regulatory Element, bGH = sequence of the polyadenylation signal of Bovine Growth Hormone gene. Gray boxes correspond to Inverted Terminal Repeats regions of AAV2.

(D) RT-qPCR on total *HTT* (*totHTT*) was performed on striatum extracts from CBA-HTT171-82Q,
20 Gfa2(B)3-HTT171-82Q and CBA/Gfa2(B)3-HTT171-82Q mice at 4, 8, 12 or 16 wpi, compared to non-injected mice (n=8-10/group, except for non-injected mice: n=5). Expression levels are normalized with Cyclophilin A levels (*Ppia*). Data represent mean ± SEM. *: $p < 0.05$, NS (Not Significant): $p \geq 0.05$, Factorial ANOVA followed by LSD Fisher Post-Hoc tests, points represent individual samples. AU = Arbitrary Units, RE = Relative Expression.

Figure 2: Behavioral alterations after mHTT expression in neurons, in astrocytes or in both cell-types.

(A) Ratio of distance traveled in the external field/the total distance traveled by the HTT171-18Q mice (gray bars) or HTT171-82Q mice (black bars) during the Open Field task (n=9-10/group). Data represent mean ± SEM. *: $p < 0.05$, Factorial ANOVA followed by LSD Fisher Post-Hoc tests, points represent individual samples.

(B) Total distance travelled was measured as an index of mouse spontaneous motor activity in the Open Field task (in meters, m, n=9-10/group). Data represent mean ± SEM. *: $p < 0.05$, Factorial ANOVA followed by LSD Fisher Post-Hoc tests, points represent individual samples.

(C) Graphic representing latency to fall (in second, sec.) of mice during Rotarod Accelerated Test n=9-10/group). Data represent mean ± SEM of the three trials of each days. *: $p < 0.05$, Repeated-Measures ANOVA followed by LSD Fisher Post-Hoc tests.

(D) Evaluation of clasping movements represented by the number of paw clasping (n=9-10/groups). Data represent mean ± SEM. *: $p < 0.05$, Factorial ANOVA followed by LSD Fisher Post-Hoc tests, points represent individual samples.

(E) Mouse body weight gain was evaluated between the surgery and euthanasia at 4, 8, 12 or 16 wpi. Data are presented in grams (g), and represent mean ± SEM. *: $p < 0.05$, Factorial ANOVA followed by LSD Fisher Post-Hoc tests, points represent individual samples.

Figure 3: mHTT aggregation patterns between striatal neurons and astrocytes

(A) Representative pictures of immunohistochemical staining of mHTT aggregates with EM48 antibody at 4, 8, 12 and 16 wpi, in the striatum of mice injected with CBA-HTT171-82Q (upper panels), Gfa2(B)3-HTT171-82Q (middle panels) or CBA/Gfa2(B)3-HTT171-82Q viral vectors (lower panels). Scale bar = 20μm (n=8-10/group).

(B) Quantifications of total number of mHTT aggregates per mm^2 after EM48 immunohistochemical staining in mouse striatum. Analysis was performed on 3 pictures/section, 3 sections/n, n=8-10/group). Data represent mean ± SEM. *: p < 0.05, Factorial ANOVA followed by LSD Fisher post-hoc tests, points represent individual samples.

5   (C) Quantifications of the number of mHTT aggregates with diameter <3μm (white bars) or ≥ 3μm (grey bars) per mm^2, after EM48 immunohistochemical staining of mouse striatum. Analysis was performed on 3 pictures/section, 3 sections/n, n=8-10/group). Data represent mean ± SEM. *: p < 0.05, Student's t tests, points represent individual samples.

(D) Immunofluorescence staining showing eGFP, HTT aggregates (Sicgen antibody) and either
10   GFAP or NeuN immunolabeling in the striatum of CBA-HTT171-82Q (right panels), Gfa2(B)3-HTT171-82Q (middle panels) and CBA/Gfa2(B)3-HTT171-82Q mice (left panels), at 16 wpi. Scale bar = 5μm.

Figure 4: Evolution of the DARPP-32 loss in mice expressing *mHTT* in neurons, in astrocytes or in both neurons and astrocytes

15   (A-B) Immunohistochemical staining of DARPP-32 protein in CBA-HTT171 (upper panels), Gfa2(B)3-HTT171 (middle panels) and CBA/Gfa2(B)3-HTT171 mice (lower panels), expressing mutant (A) or control *HTT* (B, n=8-10/group).

(C) RT-qPCR on *Ppp1r1b* mRNA performed on striatum extracts of HTT171-82Q (black bars) or HTT171-18Q (gray bars) in each model from 4 to 16 wpi (n=8-10/group). Expression levels are
20   normalized with Cyclophilin A (*Ppia*). Data represent mean ± SEM. *: p < 0.05, Factorial ANOVA followed by LSD Fisher Post-Hoc tests. AU = Arbitrary Units, RE = Relative Expression.

Figure 5: Transcriptional and morphologic analyses of striatal astrocytes

(A) RT-qPCR on *Gfap* mRNA performed on mouse striatum between mice expressing HTT171-82Q (black bars) and HTT171-18Q (gray bars) at 4, 8, 12 or 16 wpi (n=7-10/group). Expression levels are normalized with Cyclophilin A (*Ppia*). Data represent mean ± SEM, Factorial ANOVA followed by LSD Fisher Post-Hoc tests. AU = Arbitrary Units, RE = Relative Expression.

5 (B) Quantifications of labeling integrated density in Gfap-positive cells after immunohistochemical staining of mouse striatum at 16 wpi. Analysis was performed on 6 pictures/section, 3 sections/n, n=8-10/group). Data represent mean ± SEM. *: $p < 0.05$, Student's t tests.

(C) Quantifications of the total area occupied by Gfap-positive cells after immunohistochemical
10 staining of mouse striatum at 16 wpi (data are expressed in μm^2). Analysis was performed on 6 pictures/section, 3 sections/n, n=8-10/group). Data represent mean ± SEM. *: $p < 0.05$, Student's t tests.

(D) Representative pictures of immunohistochemical Gfap staining in the striatum of CBA/Gfa2(B)3-HTT171-82Q mice (left panel) and CBA/Gfa2(B)3-HTT171-18Q mice (right
15 panel). Black arrows show GFAP-positive astrocytes. Scale bar = 20μm.

Figure 6: Analysis of transcriptional dysfunctions in glutamate-glutamine cycle key elements caused by neuronal or astrocytic *mHTT*

(A-D) *Slc1a2* (Glt1, A), *Slc1a3* (Glast, B), *Atp1a2* (C) and *Glul* (Gs, D) mRNA levels were evaluated in striatum extracts of mice injected with CBA-HTT171 (upper panels), Gfa2(B)3-
20 HTT171 (middle panels) or CBA/Gfa2(B)3-HTT171 (lower panels) viral vectors. Black bars represent mice expressing *mHTT* (HTT171-82Q) and grey bars represent control groups (HTT171-18Q). All expression levels are normalized with Cyclophilin A (*Ppia*). Data represent mean ± SEM. *: $p < 0.05$, #: p=0.051 or 0.052. Factorial ANOVA followed by LSD Fisher Post-

Hoc tests (n=6-10/group). AU = Arbitrary Units, RE = Relative Expression, GOI = Gene of

Interest.

(E) Quantification of Glt1 protein levels after immunoblots on striatal extracts and normalization

with the total protein content (n=6-9/group). Data represent mean ± SEM. *: $p < 0.05$, Student's t

5   tests.

(F-G) *Grin1* (F) and G*rin2b* (G) mRNA levels were evaluated in striatum extracts of mice injected

with CBA-HTT171 (left panels), Gfa2(B)3-HTT171 (middle panels) or CBA/Gfa2(B)3-HTT171

(right panels) viral vectors. All expression levels are normalized with Cyclophilin A (*Ppia*). Data

represent mean ± SEM. *: $p < 0.05$, NS: $p \geq 0.05$, Factorial ANOVA followed by LSD Fisher

10   Post-Hoc tests (n=6-10/group). AU = Arbitrary Units, RE = Relative Expression.

Figure 7: Heat maps of correlation analyses between behavioral performances and mRNA levels

(A-C) Heat maps representing positive (red scale) and negative (blue scale) Pearson

correlations between behavioral scores and mRNA expression levels of DARPP-32 (red),

Glutamate/Glutamine cycle (Glut./glu, green), NMDAR (clear gray) or astrogliosis (GFAP, dark

15   gray) in CBA-HTT171 (A), Gfa2(B)3-HTT171 (B), or CBA/Gfa2(B)3-HTT171 mice (C). Analysis

was performed in each model separately, both on HTT171-82Q and HTT171-18Q mice at all

time points. Numbers represent R score. Yellow numbers represent FDR < 0.05, Pearson

correlations followed by *p. value* corrected for False Discovery Rate (n=37-40/group).

Figure 8: Graphical representation of the progression of each HD mouse model

20   (A-C) Schematic representation of neuronal (A), astrocytic (B) or double (C) mouse models, at 4,

8, 12 and 16 wpi (x-axis). Blue lines represent behavioral dysfunctions, red lines represent

typical HD pathological hallmarks, and green lines represent transcriptional dysfunctions of

Glutamate/Glutamine cycle elements. The absence or the intensity of dysfunctions is
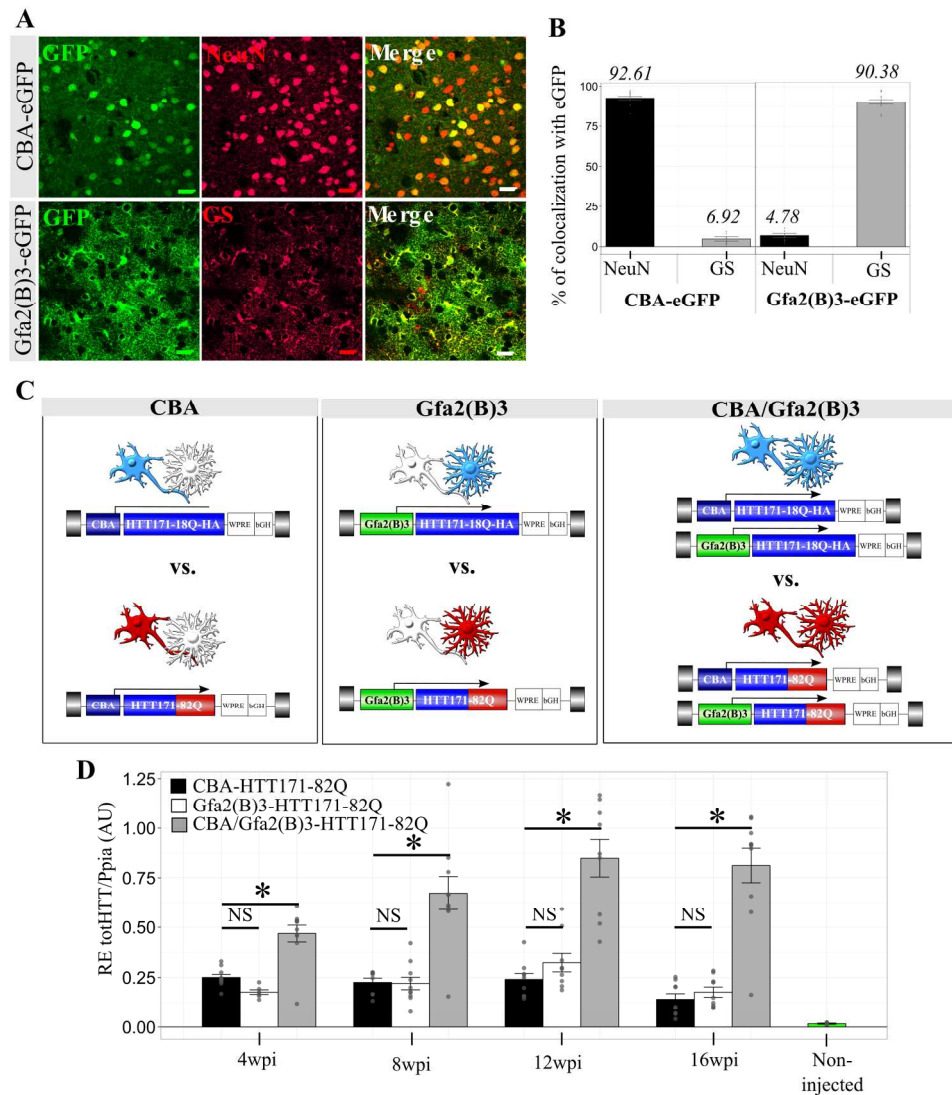
represented in the y-axis.

Figure 1: Characterization of human HTT expression induced by cell-type specific AAV2/5
(A) Representative confocal pictures of mouse striatum 3 weeks post injection of CBA-eGFP (upper panels) or Gfa2(B)3-eGFP AAV2/5 (lower panels). In CBA-eGFP mice, co-immunolabeling with a neuronal marker (NeuN, Neuronal nuclei) was performed, whereas in Gfa2(B)3-eGFP a co-immunolabeling with Glutamine Synthetase (GS), a marker of astrocytes, was performed. Scale bar = 20µm.
(B) Quantifications of the percentage of eGFP-positives cells that co-localized with NeuN or with GS, three weeks after injection of CBA-eGFP or Gfa2(B)3-eGFP AAV2/5 in mouse striatum. Data are presented as mean ± SEM, quantifications were performed on 4-6 pictures/section, 4 sections/n, n= 4.
(C) AAV2/5 vectors allowed expression of either control HTT171-18Q-HA (blue cells) or mutant HTT171-82Q (red cells), in neurons (CBA), in astrocytes (Gfa2(B)3), or in both neurons and astrocytes (CBA/Gfa2(B)3), depending on the promoter. Forty mice/group were used in each experimental condition.. WPRE = Woodchuck Post-Regulatory Element, bGH = sequence of the polyadenylation signal of Bovine Growth Hormone gene. Gray boxes correspond to Inverted Terminal Repeats regions of AAV2.
(D) RT-qPCR on total HTT (totHTT) was performed on striatum extracts from CBA-HTT171-82Q, Gfa2(B)3-HTT171-82Q and CBA/Gfa2(B)3-HTT171-82Q mice at 4, 8, 12 or 16 wpi, compared to non-injected mice (n=8-10/group, except for non-injected mice: n=5). Expression levels are normalized with Cyclophilin A levels (Ppia). Data represent mean ± SEM. *: $p < 0.05$, NS (Not Significant): $p \geq 0.05$, Factorial ANOVA

followed by LSD Fisher Post-Hoc tests, points represent individual samples. AU = Arbitrary Units, RE = Relative Expression.
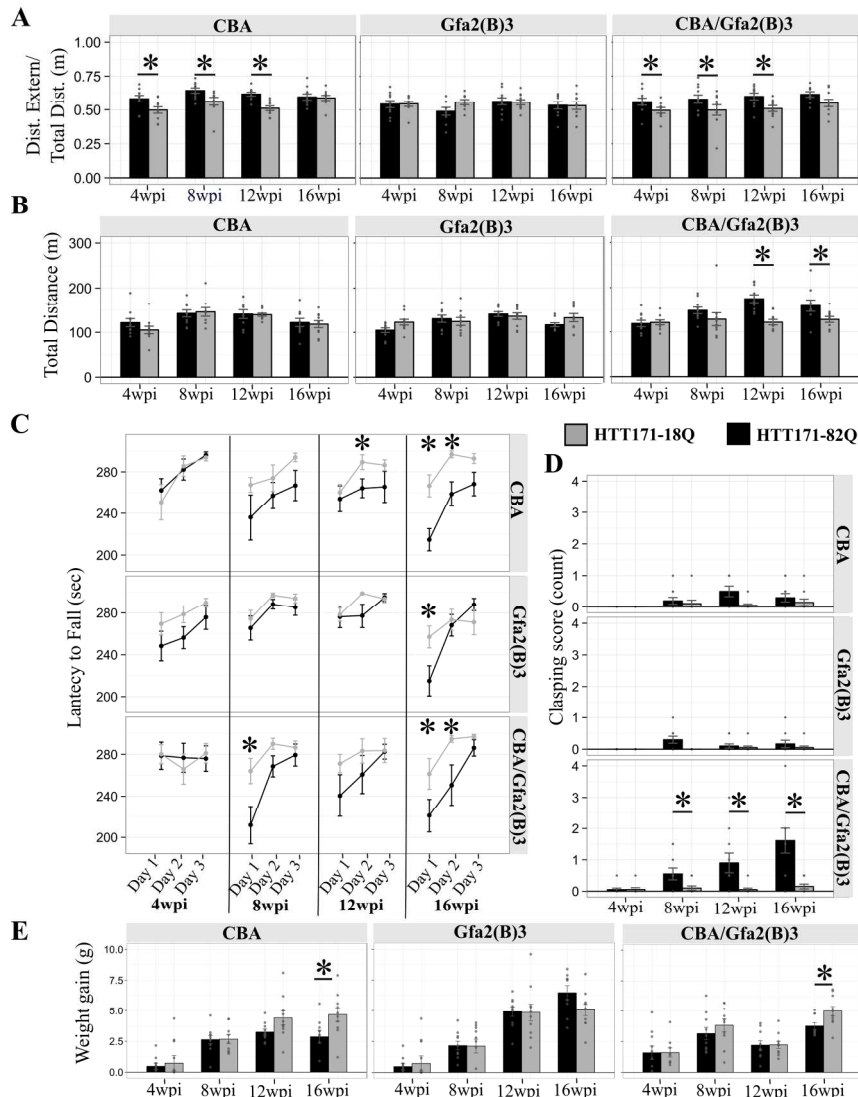
Figure 2: Behavioral alterations after mHTT expression in neurons, in astrocytes or in both cell-types.
(A) Ratio of distance traveled in the external field/the total distance traveled by the HTT171-18Q (gray bars) or HTT171-82Q mice (black bars) during the Open Field task (n=9-10/group). Data represent mean ± SEM. *: $p < 0.05$, Factorial ANOVA followed by LSD Fisher Post-Hoc tests, points represent individual samples.
(B) Total distance travelled was measured as an index of mouse spontaneous motor activity in the Open Field task (in meters, m, n=9-10/group). Data represent mean ± SEM. *: $p < 0.05$, Factorial ANOVA followed by LSD Fisher Post-Hoc tests, points represent individual samples.
(C) Graphic representing latency to fall (in second, sec.) of mice during Rotarod Accelerated Test n=9-10/group). Data represent mean ± SEM of the three trials of each days. *: $p < 0.05$, Repeated-Measures ANOVA followed by LSD Fisher Post-Hoc tests.
(D) Evaluation of clasping movements represented by the number of paw clasping (n=9-10/groups). Data represent mean ± SEM. *: $p < 0.05$, Factorial ANOVA followed by LSD Fisher Post-Hoc tests, points represent individual samples.
(E) Mouse body weight gain was evaluated between the surgery and euthanasia at 4, 8, 12 or 16 wpi. Data are presented in grams (g), and represent mean ± SEM. *: $p < 0.05$, Factorial ANOVA followed by LSD Fisher Post-Hoc tests, points represent individual samples.
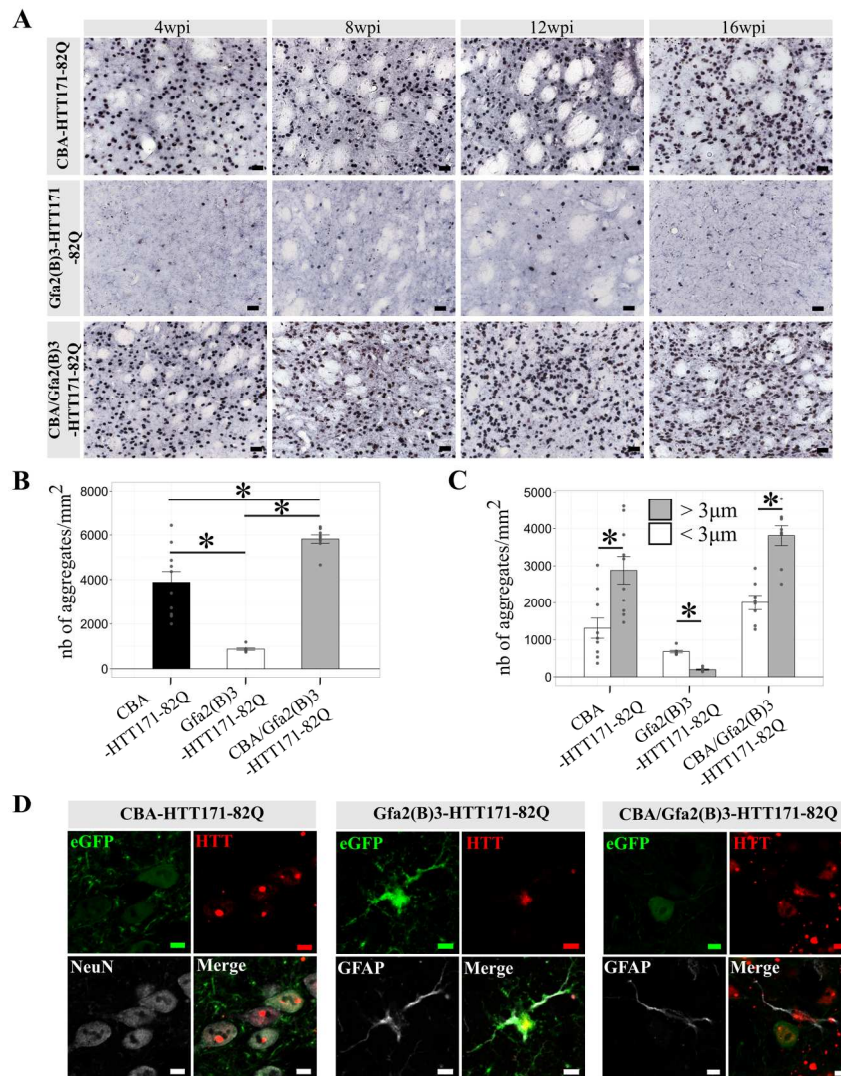
Figure 3: mHTT aggregation patterns between striatal neurons and astrocytes
(A) Representative pictures of immunohistochemical staining of mHTT aggregates with EM48 antibody at 4, 8, 12 and 16 wpi, in the striatum of mice injected with CBA-HTT171-82Q (upper panels), Gfa2(B)3-HTT171-82Q (middle panels) or CBA/Gfa2(B)3-HTT171-82Q viral vectors (lower panels). Scale bar = 20μm (n=8-10/group).
(B) Quantifications of total number of mHTT aggregates per mm2 after EM48 immunohistochemical staining in mouse striatum. Analysis was performed on 3 pictures/section, 3 sections/n, n=8-10/group). Data represent mean ± SEM. *: p < 0.05, Factorial ANOVA followed by LSD Fisher post-hoc tests, points represent individual samples.
(C) Quantifications of the number of mHTT aggregates with diameter <3μm (white bars) or ≥ 3μm (grey bars) per mm2, after EM48 immunohistochemical staining of mouse striatum. Analysis was performed on 3 pictures/section, 3 sections/n, n=8-10/group). Data represent mean ± SEM. *: p < 0.05, Student's t tests, points represent individual samples.
(D) Immunofluorescence staining showing eGFP, HTT aggregates (Sicgen antibody) and either GFAP or NeuN immunolabeling in the striatum of CBA-HTT171-82Q (right panels), Gfa2(B)3-HTT171-82Q (middle panels) and CBA/Gfa2(B)3-HTT171-82Q mice (left panels), at 16 wpi. Scale bar = 5μm.
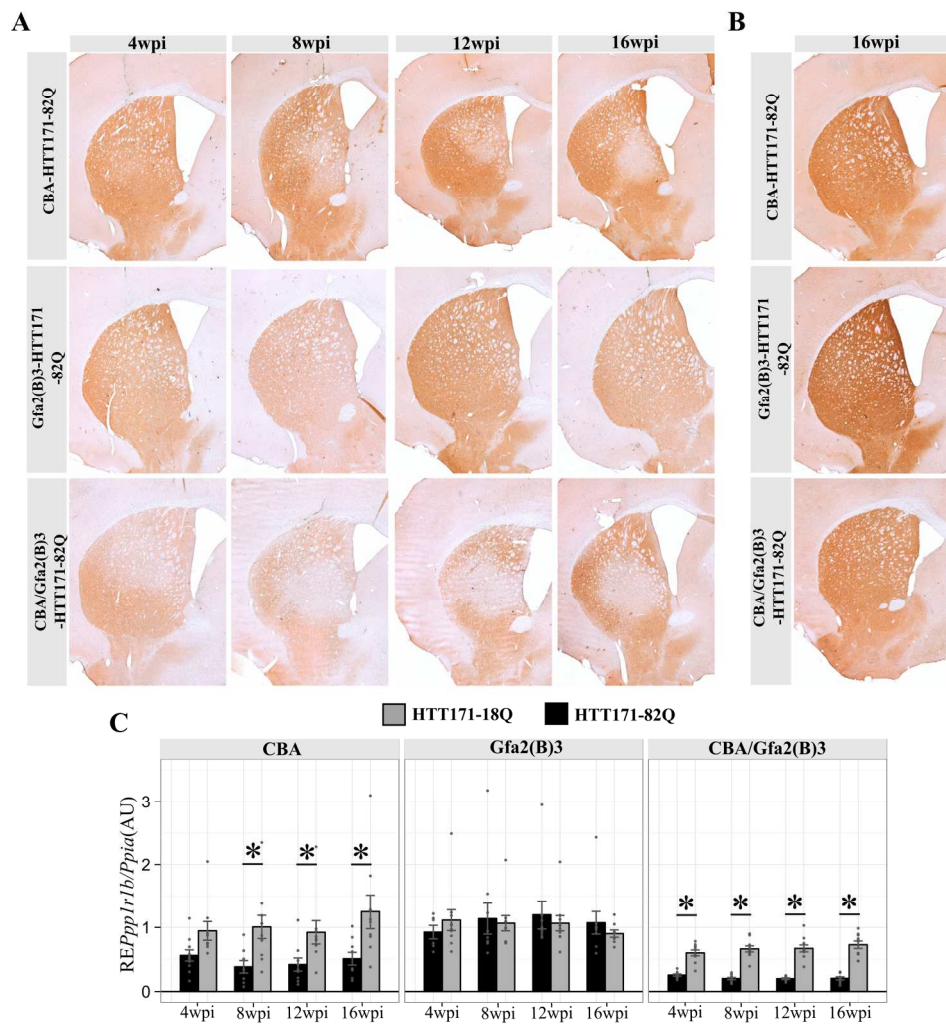
Figure 4: Evolution of the DARPP-32 loss in mice expressing mHTT in neurons, in astrocytes or in both neurons and astrocytes

(A-B) Immunohistochemical staining of DARPP-32 protein in CBA-HTT171 (upper panels), Gfa2(B)3-HTT171 (middle panels) and CBA/Gfa2(B)3-HTT171 mice (lower panels), expressing mutant (A) or control HTT (B, n=8-10/group).

(C) RT-qPCR on Ppp1r1b mRNA performed on striatum extracts of HTT171-82Q (black bars) or HTT171-18Q (gray bars) in each model from 4 to 16 wpi (n=8-10/group). Expression levels are normalized with Cyclophilin A (Ppia). Data represent mean ± SEM. *: $p < 0.05$, Factorial ANOVA followed by LSD Fisher Post-Hoc tests. AU = Arbitrary Units, RE = Relative Expression.
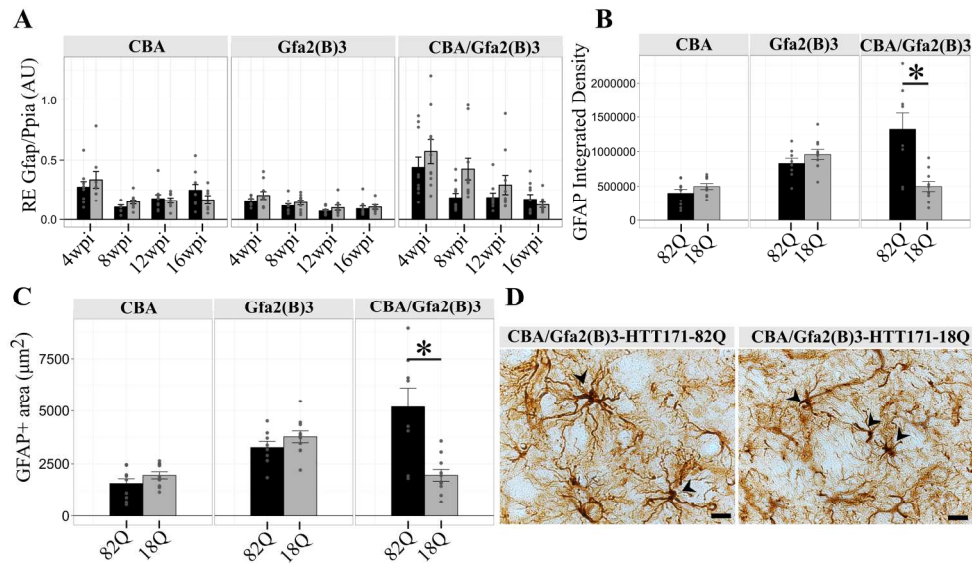
Figure 5: Transcriptional and morphologic analyses of striatal astrocytes
(A) RT-qPCR on Gfap mRNA performed on mouse striatum between mice expressing HTT171-82Q (black bars) and HTT171-18Q (gray bars) at 4, 8, 12 or 16 wpi (n=7-10/group). Expression levels are normalized with Cyclophilin A (Ppia). Data represent mean ± SEM, Factorial ANOVA followed by LSD Fisher Post-Hoc tests. AU = Arbitrary Units, RE = Relative Expression.
(B) Quantifications of labeling integrated density in Gfap-positive cells after immunohistochemical staining of mouse striatum at 16 wpi. Analysis was performed on 6 pictures/section, 3 sections/n, n=8-10/group). Data represent mean ± SEM. *: $p < 0.05$, Student's t tests.
(C) Quantifications of the total area occupied by Gfap-positive cells after immunohistochemical staining of mouse striatum at 16 wpi (data are expressed in µm2). Analysis was performed on 6 pictures/section, 3 sections/n, n=8-10/group). Data represent mean ± SEM. *: $p < 0.05$, Student's t tests.
(D) Representative pictures of immunohistochemical Gfap staining in the striatum of CBA/Gfa2(B)3-HTT171-82Q mice (left panel) and CBA/Gfa2(B)3-HTT171-18Q mice (right panel). Black arrows show GFAP-positive astrocytes. Scale bar = 20µm.
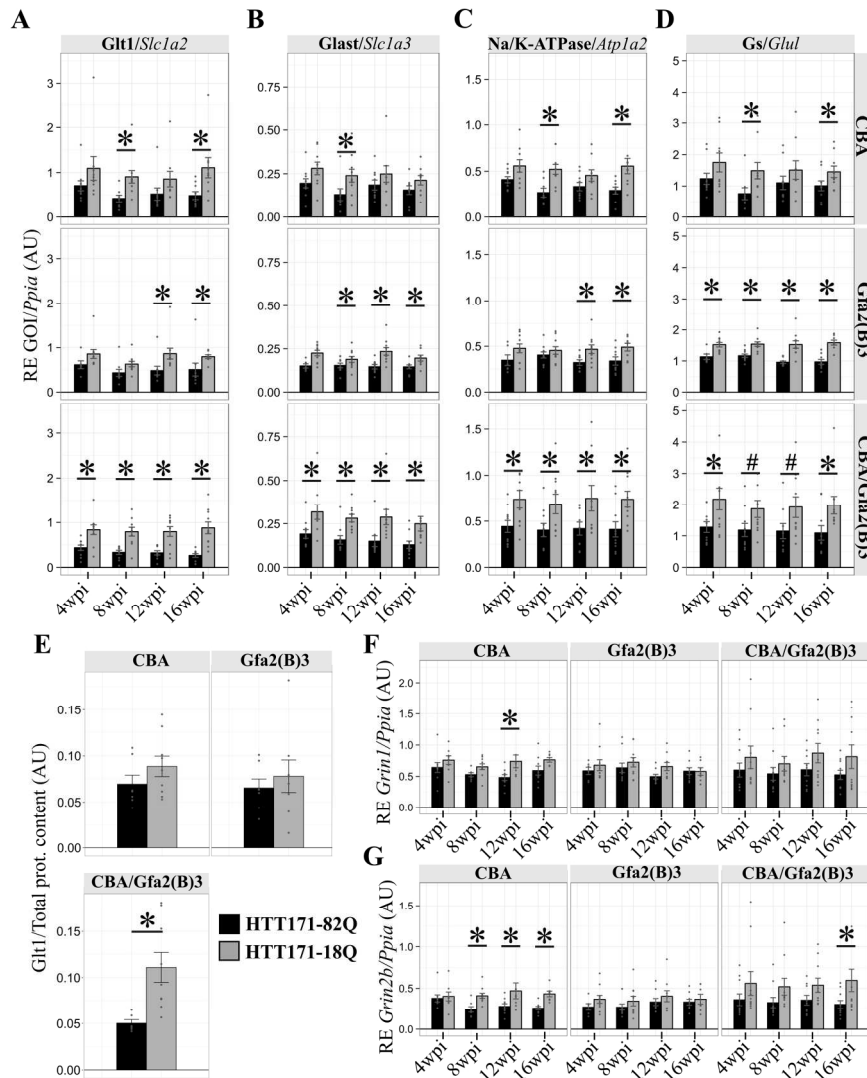
Figure 6: Analysis of transcriptional dysfunctions in glutamate-glutamine cycle key elements caused by neuronal or astrocytic mHTT
(A-D) Slc1a2 (Glt1, A), Slc1a3 (Glast, B), Atp1a2 (C) and Glul (Gs, D) mRNA levels were evaluated in striatum extracts of mice injected with CBA-HTT171 (upper panels), Gfa2(B)3-HTT171 (middle panels) or CBA/Gfa2(B)3-HTT171 (lower panels) viral vectors. Black bars represent mice expressing mHTT (HTT171-82Q) and grey bars represent control groups (HTT171-18Q). All expression levels are normalized with Cyclophilin A (Ppia). Data represent mean ± SEM. *: $p < 0.05$, #: $p = 0.051$ or 0.052. Factorial ANOVA followed by LSD Fisher Post-Hoc tests (n=6-10/group). AU = Arbitrary Units, RE = Relative Expression, GOI = Gene of Interest.
(E) Quantification of Glt1 protein levels after immunoblots on striatal extracts and normalization with the total protein content (n=6-9/group). Data represent mean ± SEM. *: $p < 0.05$, Student's t tests.
(F-G) Grin1 (F) and Grin2b (G) mRNA levels were evaluated in striatum extracts of mice injected with CBA-HTT171 (left panels), Gfa2(B)3-HTT171 (middle panels) or CBA/Gfa2(B)3-HTT171 (right panels) viral vectors. All expression levels are normalized with Cyclophilin A (Ppia). Data represent mean ± SEM. *: $p < 0.05$, NS: $p \geq 0.05$, Factorial ANOVA followed by LSD Fisher Post-Hoc tests (n=6-10/group). AU = Arbitrary Units, RE = Relative Expression.
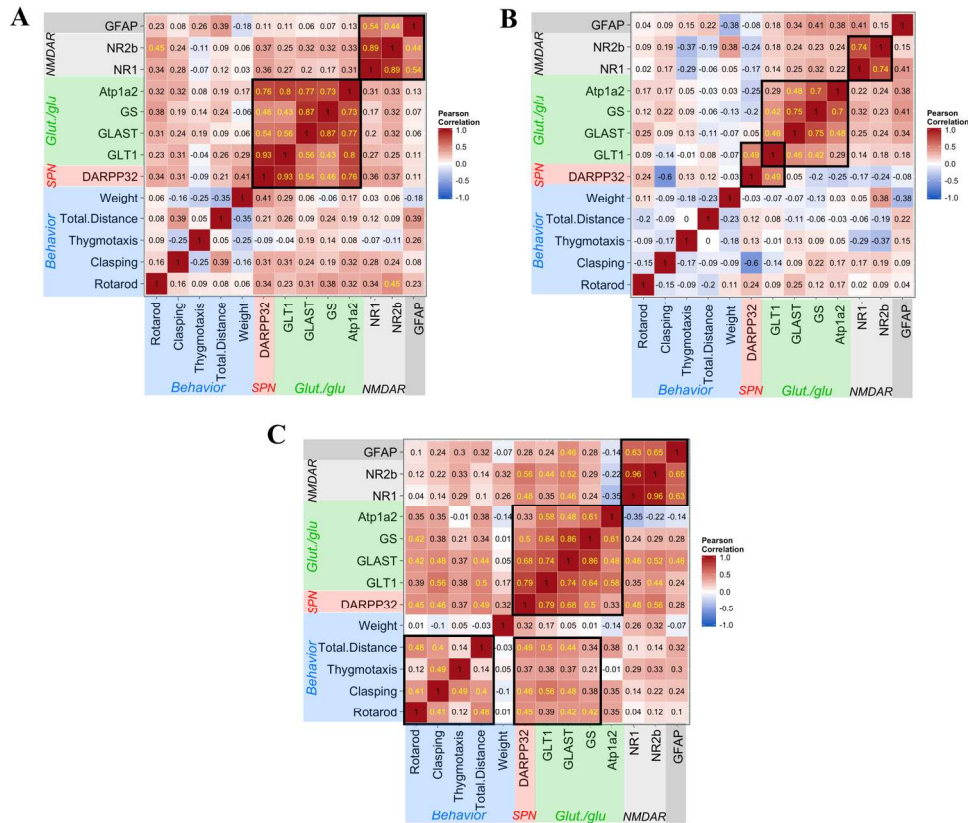
Figure 7: Heat maps of correlation analyses between behavioral performances and mRNA levels
(A-C) Heat maps representing positive (red scale) and negative (blue scale) Pearson correlations between
behavioral scores and mRNA expression levels of DARPP-32 (red), Glutamate/Glutamine cycle (Glut./glu,
green), NMDAR (clear gray) or astrogliosis (GFAP, dark gray) in CBA-HTT171 (A), Gfa2(B)3-HTT171 (B), or
CBA/Gfa2(B)3-HTT171 mice (C). Analysis was performed in each model separately, both on HTT171-82Q
and HTT171-18Q mice at all time points. Numbers represent R score. Yellow numbers represent FDR < 0.05,
Pearson correlations followed by p. value corrected for False Discovery Rate (n=37-40/group).
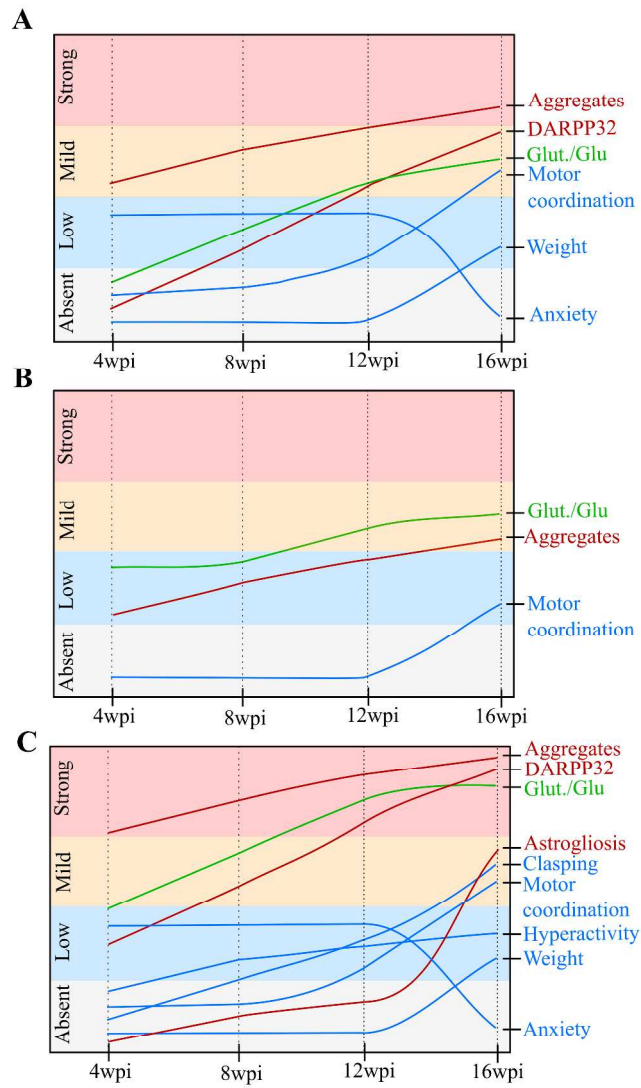
Figure 8: Graphical representation of the progression of each HD mouse model
(A-C) Schematic representation of neuronal (A), astrocytic (B) or double (C) mouse models, at 4, 8, 12 and 16 wpi (x-axis). Blue lines represent behavioral dysfunctions, red lines represent typical HD pathological hallmarks, and green lines represent transcriptional dysfunctions of Glutamate/Glutamine cycle elements. The absence or the intensity of dysfunctions is represented in the y-axis.

Supplemental Experimental Procedures – See also Experimental Procedures

Animals

Males C57Bl/6RJ mice were provided by Janvier Labs (Le Genest-Saint-Isle, France) at 10 weeks old. Mice were housed in large plastic cages containing one grid, one house, two tunnels and tree towels (cage size = 916 cm^2, 5mice/cage), in temperature controlled environment (22±1°C) on a 12hr light/dark cycle. All mice were individually handled twice per weeks, and cages were changed once per week by the same experimentator. In case of aggressiveness in 82Q groups, mice were isolated in separate cage. To avoid potential isolation effect on behavioral tests, the same number of mice from 18Q group was isolated. Food and water were provided *ad libitum*.

Plasmids cloning and AAVs production

Plasmids:

Plasmid containing Gfa2(B)3 promoter was kindly provided by Dr. Michael Brenner through the support of NIH grant NS39055. Cassette encoding Gfa2(B)3 (2.2kb, (de Leeuw et al., 2006) was removed from pUC-Gfa2(B)3-nls-LacZ and subsequently cloned into pAAV2aa-ITR-GfaABC1D-RFA-WPRE-bGH-ITR to obtain pAAV2ss-ITR-Gfa2(B)3-RFA-WPRE-bGH-ITR plasmid. Plasmids pENTR4-HTT171-18Q-HA and pENTR4-HTT171-82Q were already available in the laboratory (De Almeida et al., 2002). Gateway LR Clonase® reaction (Invitrogen, ThermoFisher Scientific, ref. 11791-019) was performed to insert HTT171-82Q, HTT171-18Q-HA , mCherry or eGFP (Clonetech, Saint-Germain-en-Laye, France) cassettes from pENTR4 plasmids into destination vectors. Final products generated were as follow: pAAV2ss-ITR-Gfa2(B)3-eGFP-WPRE-bGH-ITR, pAAV2ss-ITR-Gfa2(B)3-HTT171-82Q-HA-WPRE-bGH-ITR, pAAV2ss-ITR-Gfa2(B)3-HTT171-18Q-HA-WPRE-bGH-ITR, pAAV2ss-ITR-CBA-eGFP-WPRE-bGH-ITR, pAAV2ss-ITR-CBA-HTT171-82Q-HA-WPRE-bGH-ITR, pAAV2ss-ITR-CBA-HTT171-18Q-HA-WPRE-bGH-ITR and pAAV2ss-ITR-CBA-mCherry-WPRE-bGH-ITR respectively.

AAVs production:

AAVs were produced in HEK293T cells (mycoplasma negative, ATCC, LGC Standards GmbH). pDG5rs-Cap-Rep (Rep-Cap-Helper; Plasmid Factory, Bielefeld, Germany) and pAAV2ss containing the transgene of interest were transfected by calcium phosphate precipitation. Cells and supernatant were harvested 72h post-transfection and centrifuged at 300g for 10 minutes at 4°C. Supernatant was supplemented with 8% PEG (Sigma-Aldrich, Buchs, Switzerland) 2.5M NaCl (Merck, Nottingham, UK) and was kept at 4°C for at least 2 hours. Cell pellets were pooled and incubated in lysis buffer (NaCl 0.15M, Merck, Nottingham, UK, Tris-HCl 50mM, pH 8.5, Sigma-Aldrich, Buchs, Switzerland) for 3 consecutive freeze/thaw cycles (30 minutes in dry ice/ethanol followed by 30 minutes at 37°C). PEG-containing supernatant was centrifuged at 4'000 g for 20 minutes at 4°C after the 2 hours incubation and supernatant was discarded. Cell lysate was added to the pellets and the mixture was incubated at 37°C for 1 hour to ensure full homogenization of pellets. Lysate was then treated with benzonase (0.15 units, Sigma-Aldrich, Buchs, Switzerland) in filtered MgCl2 1M at 37°C for 30 minutes (Sigma-Aldrich, Buchs, Switzerland). Treated lysate was clarified by centrifugation at 4'000 g for 20 minutes at 4°C. AAV were separated using iodixanol (AxonLab, Le Mont sur Lausanne, Switzerland) gradient ultracentrifugation at 59'000 rpm (70Ti rotor, Beckman-Coulter, Nyon, Switzerland) for 90 minutes at 20°. Phase containing AAV was harvested and loaded on an Amicon Ultra-15 PL 100 column (Millipore, Zug, Switzerland) with 0.001% Pluronic F68 D-PBS (Gibco, ThermoFisher Scientific, Waltham, USA, Zug, Switzerland) for iodixanol cleaning and viral particles concentration. Tubes were first centrifuged at 4'000 g at 4°C until the whole solution has passed through the column. Two additional wash with 0.001% Pluronic F68 D-PBS were done and AAV were finally suspended in 250-500µL 0.001% Pluronic F68 D-PBS. The viral genomes content (vg/ml) of each AAV2/5 was assessed by Taqman® qPCR with primers recognizing Inverted Terminal Repeats of AAV2 viral genome (primer forward: 5'- GGAACCCCTAGTGATGGAGTT-3', primer reverse: 5'-CGGCCTCAGTGAGCGA-3', Taqman® probe: 5'-CACTCCCTCTCTGCGCGCTCG-3'). The titers of the different batches were as follow: AAV2/5-CBA-eGFP: 1.8E10^{11}vg/ml; AAV2/5-CBA-mCherry: 3.7E10^{11}vg/ml; AAV2/5-CBA-HTT171-18Q: 8.3E10^{10}vg/ml; AAV2/5-CBA-HTT171-82Q: 3.5E10^{11}vg/ml; AAV2/5-Gfa2(B)3-eGFP: 1.4E10^{10}vg/ml; AAV2/5-Gfa2(B)3-HTT171-18Q: 8.5E10^{11}vg/ml; AAV2/5-Gfa2(B)3-HTT171-82Q: 2.1E10^{12}vg/ml. AAV2/5 vectors were stored at -80°C until use.

Injections

Stereotaxic surgeries:

Surgeries were performed at 11 weeks old. Mice were randomly assigned to experimental groups. Mice were anesthetized with intra-peritoneal injection of a mix of Ketamine (100mg/kg, Ketasol ®, Graeub, Bern, Switzerland) and Xylazine (10mg/kg, Rompun ®, Bayer Health Care, Uznach, Switzerland) in Sodium Chloride 0.9% (NaCl, B-BRAUN, Melsungen, Germany). The head of the mouse was shaved, and the animal was placed on the stereotaxic frame (Model 963 Ultra Precise Small Animal Stereotaxic Instrument, Kopf, Tujunga, USA). The mouse temperature was monitored and kept constant (>36°C), and Viscotears ® (Swissmedic, Bern, Switzerland) was continuously applied on eyes to avoid drying. Liquid Betadine ® was applied to clean the skin before incision and exposure of the skull. A 25G needle fixed to a syringe holder was used to pierce the skull at appropriate coordinates. All injections were performed bilaterally. For tropism validation, CBA-eGFP and Gfa2(B)3-eGFP viral vectors were injected in one site/hemisphere (AP: +1 ; ML: ±1.5 ; DV: -3.5). For diffusion analysis, CBA-mCherry and Gfa2(B)3-eGFP vectors were co-injected in two sites/hemisphere (anterior striatum = AP: +1 ; ML: ±1.5 ; DV: -3.5 ; posterior striatum = AP: 0 ; ML: ±2 ; DV: -3.5). For neuron or astrocyte specific HD mouse models, CBA-HTT171-82Q, CBA-HTT171-18Q, Gfa2(B)3-HTT171-82Q or Gfa2(B)3-HTT171-18Q viral vectors were injected with either CBA-eGFP or Gfa2(B)3-eGFP vectors in two sites/hemisphere. For CBA/Gfa2(B)3-HTT171 mice, CBA-HTT171-82Q and Gfa2(B)3-HTT171-82Q, or CBA-HTT171-18Q and Gfa2(B)3-HTT171-18Q vectors were co-injected, together with CBA-eGFP viral vectors. Viral vectors were injected with 34G steel cannulas (Unimed, Lausanne, Switzerland) fixed on a cannula holder and linked to an 10μl Hamilton syringe and an infusion pump (CMA 4004, Phymep, Paris, France). For each site, 2μl of viral vector was injected at 0.2μl/min. Cannulas were left in the brain for 5 minutes after injection, and then slowly removed. Skin was closed using 6.0 sterile suture thread (Novosyn DS12, B-BRAUN, Melsungen, Germany). Sterile NaCl 0.9% solution was delivered to the mouse by sub-cutaneous injection to avoid dehydration after surgery, and healing cream (Bepanthen®Plus, BAYER, Leverkusen, Germany) was applied on the head. Sugar-taste Paracetamol (Dafalgan ®, UPSA, Agen, France) was delivered to the mice in water (500mg/cage) during 72h. Mice were monitored until complete awakening, and every day during three days after surgery.

Viral vectors doses:

All viral vectors were injected in a final volume of 2μl/sites. For tropism study, CBA-eGFP was injected at $5E10^7$ viral genomes (vg)/sites. Due to low viral titer, Gfa2(B)3-eGFP vector was injected at $2.75E10^7$ vg/site. To evaluate the diffusion of AAV2/5 in basal ganglia circuit, we co-injected CBA-mCherry and Gfa2(B)3-eGFP at $5E10^7$ vg/sites per viral vector. AAV2/5 containing CBA-HTT171 were co-injected with AAV2/5 containing CBA-eGFP at $5E10^7$ vg/site and $4E10^6$ vg/sites respectively. AAV2/5 containing Gfa2(B)3-HTT171 were co-injected with AAV2/5 containing Gfa2(B)3-eGFP at $5E10^7$ vg/site and $4E10^6$ vg/sites respectively. The co-injection of CBA-HTT171-82Q and Gfa2(B)3-HTT171-82Q, or CBA-HTT171-18Q and Gfa2(B)3-HTT171-18Q were performed with $5E10^7$ vg/sites/viral vector, in combination with $4E10^6$ vg/site of CBA-eGFP vector.

Behavioral tests

Each mouse was habituated to the room and to the experimentator by individual handling during 1min./day during three days before behavioral tests. The total duration of tests was one week, in the following order: Open Field, Rotarod Accelerated test, Clasping test, weight follow-up, EchoMRI.

Open Field

Mouse was placed in the center of a circular gray arena (diameter = 75 cm, home-made) and was free to explore during 30 min. Automated recording of mouse movements were performed using video camera coupled to tracking analysis by Anymaze © software (software available on: http://www.anymaze.com/). Extern field correspond to a 10 cm band along the walls, and Intern field was all the remaining area. We analyzed the total distance traveled by the mouse, and the distance traveled in extern field of the arena.

Rotarod Accelerated Test

Rotarod Accelerated test was performed on UGO-BASILE apparatus (model 7600, Ugo-Basile, Comerio-Varese, Italy), consisting of five equal compartments on a plastic-gripped cylinder. Groups of mice evaluated at the same time were kept constant to avoid increased anxiety. Mice were first trained during 5min. at 4 rotations per minutes

(rpm) for habituation. Tests were conducted during three trials per days (with 45 min. resting between each trial) during three consecutive days. For each trial, mice were placed on the rod that accelerate from 4 to 40 rpm in 5 min. Latency to fall (or if mice hung on for more than two consecutive rotations without running) was recorded.

Clasping Test

Mice were individually suspended by the experimentator at the last third of the tail during 30 sec., at 1.5 m. from the floor. Two blind observers rated the number of paw clasping, corresponding to the clasping score (1 = one anterior paw, 2 = two anterior paws, 3 = two anterior paws and one posterior paw, 4 = four paws, adapted from Fink et al., 2013).

Weight follow-up and EchoMRI

Mice were weighted the day of the surgery and the day before euthanasia at 4, 8, 12 or 16 wpi. The weight difference between the two time-points was considered as the weight gain. Whole body composition analysis was performed with EchoMRI ® Analyzer (Houston, USA). We measured the whole body masses of fat and lean.

Cell cultures and transfections

HEK293T cells were cultured in DMEM medium (Gibco, ThermoFisher Scientific, Waltham, USA, ref. 32430027), completed with 10% Fetal Bovine Serum (Gibco, ThermoFisher Scientific, Waltham, USA, ref. 10270-106) and 1% of Peniciline-Streptomycin (Gibco, ThermoFisher Scientific, Waltham, USA, ref. 15140-122). pAAV2ss CBA-HTT171-82Q and CBA-HTT171-18Q-HA plasmids were transfected by calcium-phosphate precipitation. HEPES buffer (Sigma-Aldrich, Buchs, Switzerland, ref. n°51558) and 0.5M CaCl2 solution (Merck, Darmstadt, Germany, ref. TA799582) were mixed together with 4μg of plasmid (300.000 cells per well in a 6-well plate, Vitaris, Baar, Switzerland). Medium were changed 6h after transfection. Three days after transfection, cells were washed two times with HBSS (Gibco, ThermoFisher Scientific, Waltham, USA, ref. 14025092) and lysed in 1mL of TRIzol Reagent ® (Ambion, ThermoFisher Scientific, Waltham, USA, ref. 15596-026).

Brain samples processing

All procedure for brain dissection was performed under RNAse-free conditions. Mice were anesthetized by lethal i.p injection of Pentobarbital (150mg/kg, Esconarkon, Streuli Pharma, Uznach, Switzerland). After decapitation, brain was quickly removed and placed in a cold dissection matrix to isolate 1mm slices. Brain slices were placed under inverted Fluorescent Microscope (Olympus IX 81) to quickly dissect eGFP-positive area in the striatum. Punches were immediately homogenized on ice in 200μl of TRIzol Reagent® solution (Invitrogen, ThermoFisher Scientific, Waltham, USA, ref. 15596026), completed until 1ml, and stocked at -80°C.

For brain fixation, mice were anesthetized by lethal i.p injection of Pentobarbital (150mg/kg, Esconarkon, Streuli Pharma, Uznach, Switzerland). Intra-cardiac perfusion of cold Phosphate-buffered saline (PBS 1X) was performed during 1min. (20ml/min.), followed by perfusion of cold fresh Paraformaldehyde (4%) solution diluted in 0.15M Na-Phosphate buffer during 5 min (20ml/min.). Brain was next quickly dissected and post-fixed in Paraformaldehyde solution during additional 12h, followed by cryo-protection in PBS 1X-Sucrose 20% (12h) and PBS 1X-Sucrose 30% (12h). Brains were conserved at -80°C until use.

RNA and protein extraction:

RNA and protein extractions were performed according to TRIzol Reagent ® kit recommendations (Invitrogen, ThermoFisher Scientific, Waltham, USA, ref. 15596026). All extractions were performed on ice under RNAse free conditions, with ultrapure sterile RNAse-DNAse free water (Invitrogen, ThermoFisher Scientific, Waltham, USA, ref. 10977-049). HTT171-18Q and HTT171-82Q samples were extracted at the same time. Glycogen (10μg, Invitrogen, ThermoFisher Scientific, Waltham, USA, ref. 10814-010) was added before RNA extraction to improve RNA pellet visualization. RNA washes with 75% ETOH were performed twice, and pellet was finally suspended in 22μl (*in vivo* samples) or 52μl (*in vitro* samples) of ultrapure water and stored at -80°C. RNA concentration and potential chemical contaminations were evaluated by Nanodrop® (ND-1000 Spectrophotometer, Witec, Luzern, Switzerland). Samples with aberrant $A_{260/280}$ or $A_{260/230}$ ratios were discarded.

Protein extractions were performed according to TRIzol ® kit recommendations (Invitrogen, ThermoFisher Scientific, Waltham, USA, ref. 15596026). Samples were resuspended at the end of the extraction in a solution containing 2/3 SDS 1% (Invitrogen, ThermoFisher Scientific, Waltham, USA, ref. 15525-017) and 1/3 Urea 10M (Acros Organics, Geel, Belgium, ref. 327380010), at 95°C during 30min on agitation (300rpm), then stored at -20°C. Protein concentration was evaluated using Micro BCA™ Protein assay kit (ThermoFicher Scientific, Waltham, USA, ref. 23235), according to kit recommendations.

Immunohistochemistry and image acquisitions

Primary and secondary antibodies are detailed in following tables. For fluorescent labeling, 20μm free-floating sections were washed three times (10min./wash) at room temperature (RT) in PBS 1X, blocked 1h in PBS 1X containing 5% Donkey Serum (Sigma-Aldrich, Buchs, Switzerland, ref. D9663) and 0.1% Triton (Sigma-Aldrich, Buchs, Switzerland, ref. X-100). Sections were incubated overnight at 4°C in PBS 1X containing 0.1% Triton, 5% Donkey Serum and primary antibodies. The following day sections were washed three times in PBS 1X and incubated 2h in PBS 1X containing 5% Donkey Serum, 0.1% Triton and secondary antibodies. Sections were finally washed three-times in PBS 1X, incubated in Hoechst33342 trihydrochloride trihydrate solution (10μg/ml, Invitrogen, ThermoFicher Scientific, Waltham, USA, ref. H3570) during 5min at RT., rinsed three times in PBS 1X and mount on SuperFrost Ultra Plus microscope slides (ThermoFicher Scientific, Waltham, USA, ref. J3800AMNZ) in Fluoromount medium (Sigma-Aldrich, Buchs, Switzerland, ref. F4680).

For chromogen-based labeling, 20μm sections were treated with tris-buffered saline (TBS, Tris 10mM, AppliChem, Darmstadt, Germany, ref.A1087, 0.9% NaCl, Sigma-Aldrich, Buchs, Switzerland, ref. A2942) containing 3% hydrogen peroxide (Sigma-Aldrich, Buchs, Switzerland, ref. 31642) and 10% Methanol (ThermoFicher Scientific, Waltham, USA, ref. M/4058/17) during 15 min. to quench endogenous peroxidase activity. Sections were rinsed three-times in TBS, incubated 1h at RT in TBS containing 0.1% Triton and 5% of Bovine Serum Albumine Fraction V (BSA, AppliChem, Darmstadt, Germany, ref. A1391) followed by overnight incubation at 4°C in TBS containing 0.1% Triton, 1% BSA and primary antibody. The following day, sections were washed three times in TBS, incubated in TBS containing 0.1% Triton, 1% BSA and appropriate biotinylated secondary antibody during 2h at RT, and developed with avidin-biotinylated horseradish peroxidase complexes for 1h at RT (Vector Labs, Burlingame, Canada, ref. PK6200). Immunoreactivity was revealed using either nickel-amonium sulfate and diaminobenzidine (DAB, black reaction) or only DAB following kit recommendations (Vectors Labs, Burlingame, Canada, ref. SK-4100). HTT171-18Q and HTT171-82Q samples were processed in parallel with identical revelation conditions between all groups. Sections were dehydrated in ethanol followed by xylene (Sigma-Aldrich, Buchs, Switzerland, ref. X1040), and mount on Superfrost Ultra Plus microscope slides with Eukitt® medium (Sigma-Aldrich, Buchs, Switzerland, ref. 03989).

Fluorescent images were captured using inverted Zeiss LSM 510 Meta confocal microscope (Supplemental Figure 1B) or inverted Zeiss LSM 880 confocal microscope (all other fluorescent pictures). Images of DAB immunohistochemistry were captured using upright Zeiss Axio Imager.Z1. For quantitative analysis, all acquisition parameters were kept constant between samples and between groups. Quantifications of EM48-positives mHTT aggregates and Gfap-positive cells were performed manually with ImageJ 1.44p software and the Cell Counter plugin. Analysis of Integrated Density and area of Gfap immunolabeling were automatically performed with home-made macro in ImageJ 1.44p (software available on: http://imagej.nih.gov/ij/index.html). All analyses were performed on raw unmodified images. To aid visualization, some panels of DAB immunohistochemistry comprises images with subsequent adjustments of brightness and contrast made in Photoshop (CS6, Adobe, software available on: http://www.adobe.com/ch_fr/products/photoshop.html), adjustments were identical between groups.

List of primary antibodies:

Primary antibody	Host organism	Dilution	Product Reference (RRID)
GFP	Goat	1:1000	Sicgen, AB0020-200 (RRID: AB_2333099)
mCherry	Goat	1:1000	Sicgen, AB0040-200 (RRID: AB_2333092)

HTT (EM48)	Mouse	1:100	Millipore, MAB5374 (RRID: AB_10055116)
HTT (Sicgen)	Goat	1:1000	Sicgen, AB0080-200 (RRID: AB_2333150)
NeuN (Figure 1, tropism quantifications)	Mouse	1:500	Millipore, MAB377 (RRID: AB_10048713)
NeuN (Figure 4, Supplemental Figure S3 and S5)	Rabbit	1:1000	Millipore, ABN78 (RRID: AB_11211087)
GFAP	Rabbit	1:500	DakoCytomation, Z0334 (RRID: 2314535)
GS	Rabbit	1:1000	Sigma-Aldrich, G2781 (RRID: AB_259853)
DARPP-32	Rabbit	1:1000	Cell Signaling, 2302S (RRID: AB_10691682)

List of secondary antibodies:

Secondary antibody	Host organism	Dilution	Product reference (RRID)
Alexa Fluor 488 conjugated anti-goat	Donkey	1:500	Thermo Fisher Scientific, A11055 (RRID: AB_10564074)
Cy3 conjugated anti-goat	Donkey	1:500	Jackson Immunoresearch, 705-166-147 (RRID: AB_2340413)
Cy3 conjugated anti-mouse	Donkey	1:500	Jackson Immunoresearch 715-166-150 (RRID: AB_2340816)
Alexa Fluor 594 conjugated anti-rabbit	Donkey	1:500	Jackson Immunoresearch 711-586-152 (RRID: AB_2340622)
Cy5 conjugated anti-rabbit	Donkey	1:500	Jackson Immunoresearch 711-175-152 (RRID: AB_2340607)
Biotinylated anti-mouse	Horse	1:400	Vector Laboratories, BA2000 (RRID:AB_2313581)
Biotinylated anti-rabbit	Goat	1:500	Vector Laboratories, BA1000 (RRID: AB_2313606)

RT-qPCR

Primer sequences are detailed in the following table. mRNAs were treated with DNAse enzyme (220ng mRNA/reaction, RQ1 DNAse 1, Promega, Madison, USA, ref. M6101), according to kit recommendations. cDNA synthesis by reverse transcription was performed using Superscript II Reverse Transcriptase enzyme (100ng of DNAse-treated mRNA/reaction, ThermoFisher Scientific, Waltham, USA, ref. 18064-014), according to kit recommendation (0.5µM Random Hexamers, Invitrogen, ThermoFisher Scientific, Waltham, USA, ref. N8080127, and 0.1mM dNTPs, Invitrogen, ThermoFisher Scientific, Waltham, USA, ref. 18427-013). qPCR were performed using KAPA SYBR Fast kit (KAPA, Labgene Scientific, Châtel-St-Denis, Switzerland, ref.KK4602). Final mix contained 200nM of each primer, 1ng cDNA, 1X ROX High and 1X KAPA SYBR Fast (20µl of total reaction). Samples from HTT171-18Q and HTT171-82Q, or from 4, 8, 12 or 16 wpi were homogeneously divided in 96-wells qPCR plates (Applied Biosystems, ThermoFisher Scientific, Waltham, USA, ref. 4346907), to allow further statistical comparisons. Housekeeping gene (*Ppia*) was repeated in all reaction plate, to control for inter-plates repeatability. Samples were loaded in triplicate and technical replicates with variability $\geq$ 2% were discarded. Negative controls containing KAPA SYBR, primers, ROX High and water were loaded in each plate for each primer pair and melting curve analysis was performed to control for contaminations. Normalization on *Ppia* for each gene was performed for each sample, according to following formula (RE = Relative Expression, Cq = quantification cycle, GOI = Gene Of Interest):

$$RE_{GOI} = \frac{2^{Cq_{GOI}}}{2^{Cq_{Ppia}}}$$

Targeted gene:	Specie:	Primers sequences:
HTT	Human and mouse	5'-CCGCTGCACCGACCAAAGAA-3'
		3'- ATTTCTGAGAGACTGTGCCA-5'
HTT	Human	5'-CTGCACCGACCAAAGAAAGAAC-3'
		3'-CATAGCGATGCCCAGAAGTTTC-5'
ACTB	Human	5'-TGAAGGTGACAGCAGTCGGTTG-3'
		3'-GGCTTTTAGGATGGCAAGGGAC-5'
Ppia	Mouse	5'-ATGGCAAATGCTGGACCAAA-3'
		3'-GCCTTCTTTCACCTTCCCAAA-5'
Ppp1r1b	Mouse	5'-CCCTGAGCCTGGCACATAAG-3'
		3'-AAGCCGCAGCCCTAGCA-5'
Slc1a2	Mouse	5'-GGCAATCCCAAACTCAAGAAGC-3'
		3'-GTCACTGTCTGAATCTGCTGGAAAC-5'
Slc1a3	Mouse	5'-TCTCCAGTCTCGTCACAGGAATG-3'
		3'-TGCCAATCACCACAGCAATG-5'
Atp1a2	Mouse	5'-GAGACGCGCAATATCTGTTTCTT-3'
		3'-ACCTGTGGCAATCACAATGC-5'

Glul	Mouse	5'-CACCGCTCTGAACACCTTCC-3'
		3'-TGGCTTGGACTTTCTCACCC-5'
Grin1	Mouse	5'-TCCCAACGACCACTTCACTC-3'
		3'-AGTAGATGGACATTCGGGTAGTC-5'
Grin2b	Mouse	5'-GCTACAACACCCACGAGAAGAG-3'
		3'-GAGAGGGTCCACGCTTTCC-5'
Gfap	Mouse	5'-ACGACTATCGCCGCCAACT-3'
		3'-GCCGCTCTAGGGACTCGTTC-5'

Western blot

Mix containing proteins (20μg for GLT-1 blots or 30μg for HTT blots) and Laemmli buffer 1X (BIO-RAD, Cressier, Switzerland, ref. 161-0747) was heated at 95°C during 5min. for denaturation. Samples were run on SDS-PAGE on 10% acrylamide gels and transferred to 0.2μm nitrocellulose membranes (BIO-RAD, Cressier, Switzerland, ref. 1704158) with the semi-dry TransBlot-Turbo™ transfer system (BIO-RAD, Cressier, Switzerland). Non-specific binding sites were blocked for 1h at RT in tris-buffered saline (TBS, Tris-Hcl pH 7.5 50mM, NaCl 150mM) containing 0.1% Tween® (AppliChem, Darmstadt, Germany, ref. A1389) and 5% of nonfat dried milk (Applichem, Darmstadt, Germany, ref. A0830). Membranes were next incubated in TBS containing 0.1% Tween, 5% milk and primary antibody (GLT-1; Alpha Diagnostic International, ref. GLT11-A, RRID: AB_1622410, 1:500 or HTT, Sicgen, ref. AB0080-200, RRID: AB_2333150, 1:1000), at 4°C during 48h (GLT-1) or 12h (HTT). Membranes were washed three times with TBS 0.1% Tween, and incubated 2h at RT in TBS containing 0.1% Tween, 5% milk and secondary antibody (HRP-donkey anti-rabbit; GE Healthcare, ref. NA9340, RRID: AB_772191, 1:7000 or HRP-donkey anti-goat, Santa Cruz, Heildeberg, Germany, ref. sc-2056, RRID: AB_631730, 1:10.000). Blots were next washed three times in TBS 0.1% Tween and processed using Western Bright Sirius ECL kit (Advansta, Menlo Park, USA, ref. K12043-D20), according to kit recommendations. Chemiluminescence detection was performed with the ChemiDoc™ XRS System (BIO-RAD, Cressier, Switzerland, ref. 170-8070). For GLT-1 blots total protein content assay was performed with the Pierce Reversible Protein Stain kit (ThermoFicher Scientific, Waltham, USA, ref. 24580) according to kit recommendations. Both labeling were quantified with the ImageLab 3.0 (BIO-RAD, Cressier, Switzerland, software available on: http://www.bio-rad.com/en-us/product/image-lab-software), and GLT1 protein level was normalized to the total protein content.

Statistical Analysis:

Statistical analyses were performed with Statistica 10 Statsoft (DELL, software available on: http://www.statsoft.com/Products/STATISTICA-Features/Version-10). Student's t tests were performed when only two groups were compared otherwise Factorial ANOVA was applied. A repeated measure ANOVA was used for Rotarod Accelerated Test. Post-hoc LSD Fisher tests were applied after ANOVA if significant. *P value* < 0.05 was considered as significant. Pearson correlations were performed in Statistica 10 Statsoft, behavioral scores of clasping, thigmotaxis, and motor activity in the Open Field were inverted, and *p value* correction by FDR estimation was performed with R 3.1.2 and *stats* package (http://www.R-project.org), according to Benjamini and Hochberg method (Benjamini and Hochberg, 1995). Figures were realized with Inkscape 0.91 (software available on: https://inkscape.org/fr/), graphics were performed in R 3.1.2 with *ggplot2* and *grid* packages (Wickham, 2009).
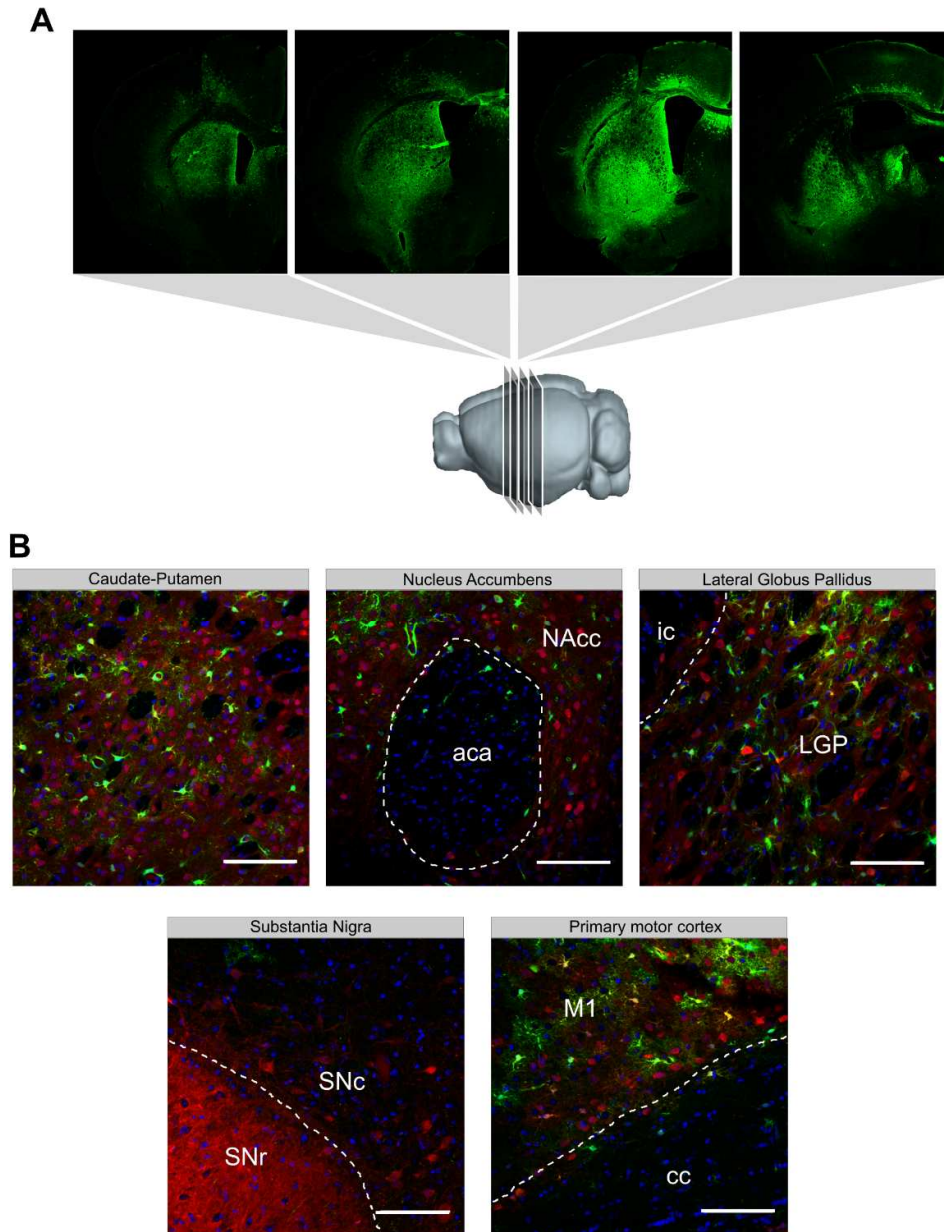
Supplemental References:

Benjamini, Y., and Hochberg, Y. (1995). Controlling the False Discovery Rate: A Practical and Powerful Approach to Multiple Testing. Journal of the Royal Statistical Society 57, 289.
Fink, K.D., Rossignol, J., Crane, A.T., Davis, K.K., Bombard, M.C., Bavar, A.M., Clerc, S., Lowrance, S.A., Song, C., Lescaudron, L., and Dunbar, G.L. (2013). Transplantation of umbilical cord-derived mesenchymal stem cells into the striata of R6/2 mice: behavioral and neuropathological analysis. Stem cell research & therapy 4, 130.
Wickham, H. (2009). ggplot2: Elegant Graphics for Data Analysis, 1 edn (New York: Springer-Verlag New York).

Figure S1: Analysis of transgene expression in the basal ganglia circuit after injection of AAV2/5 in the mouse striatum.
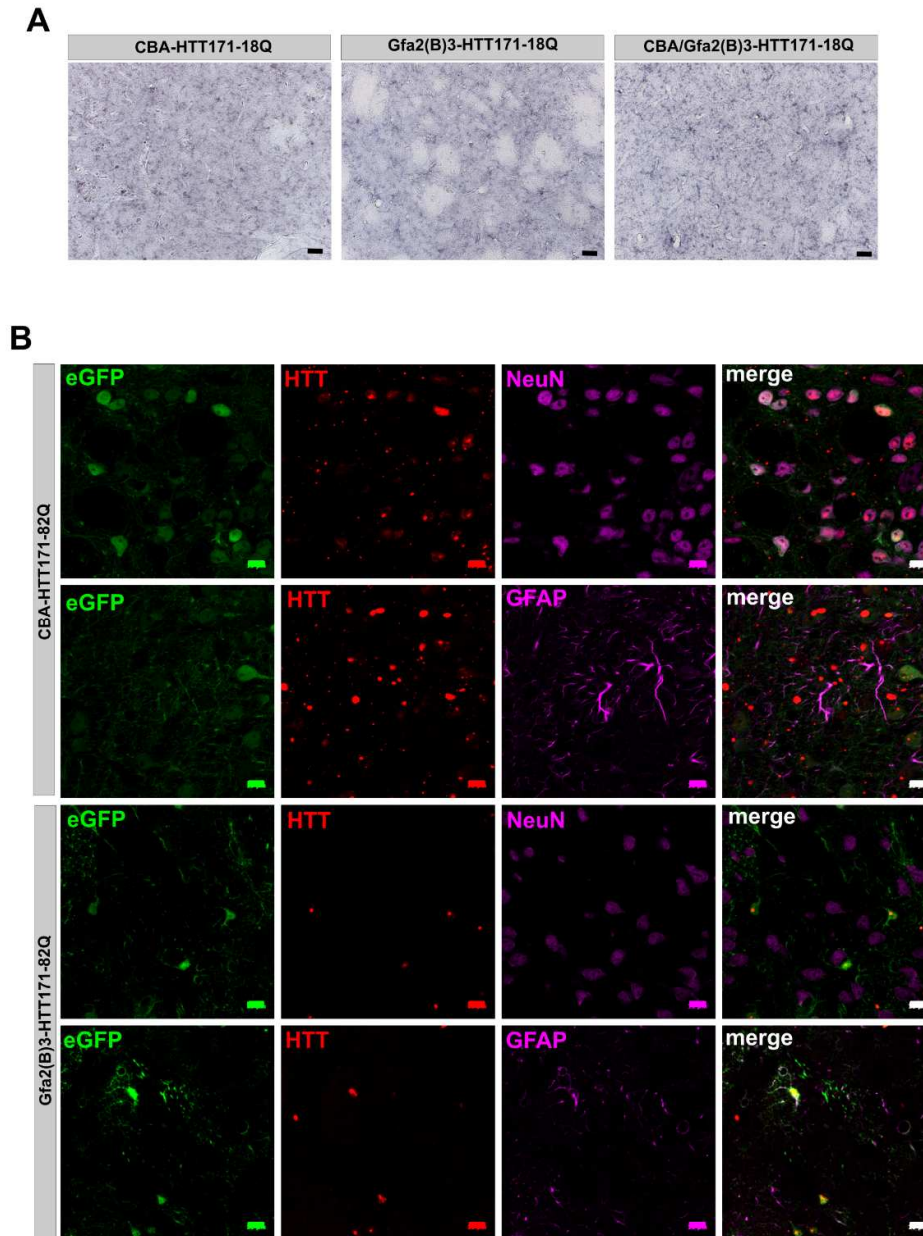

(A) Mosaic acquisitions of mouse striatum 3 weeks after injection of CBA-eGFP in two sites per hemispheres ($5E10^7$ viral genome/site). Immunohistochemistry against eGFP was performed. Expression of eGFP was detected in large part of the striatum, both in medio-lateral and anterior-posterior axes. Brain 3D representation was exported from Brain Explorer 2 software (Allen Institute for Brain Science, Seattle (WA), available from: http://human.brain-map.org/static/brainexplorer).

(B) Pictures of distinct structures of the mouse basal ganglia system three weeks after co-injection of CBA-mCherry and Gfa2(B)3-eGFP AAV2/5 in two sites per hemisphere ($5E10^7$ viral genomes/sites per viral vector). mCherry-positive and eGFP-positive cell were detected in the Caudate-Putamen, the Nucleus Accumbens (NAcc), the Lateral Globus Pallidus (LGP), the substantia nigra and the primary motor cortex (M1). Scale bar = 100µm. aca = anterior commissure anterior part, ic = internal capsule, SNr = substantia nigra pars reticulata, SNc = substantia nigra pars compacta, cc = corpus collosum. To

help visualization, acquisition parameters differs between structures due to high heterogeneity in eGFP and/or mCherry expression levels.
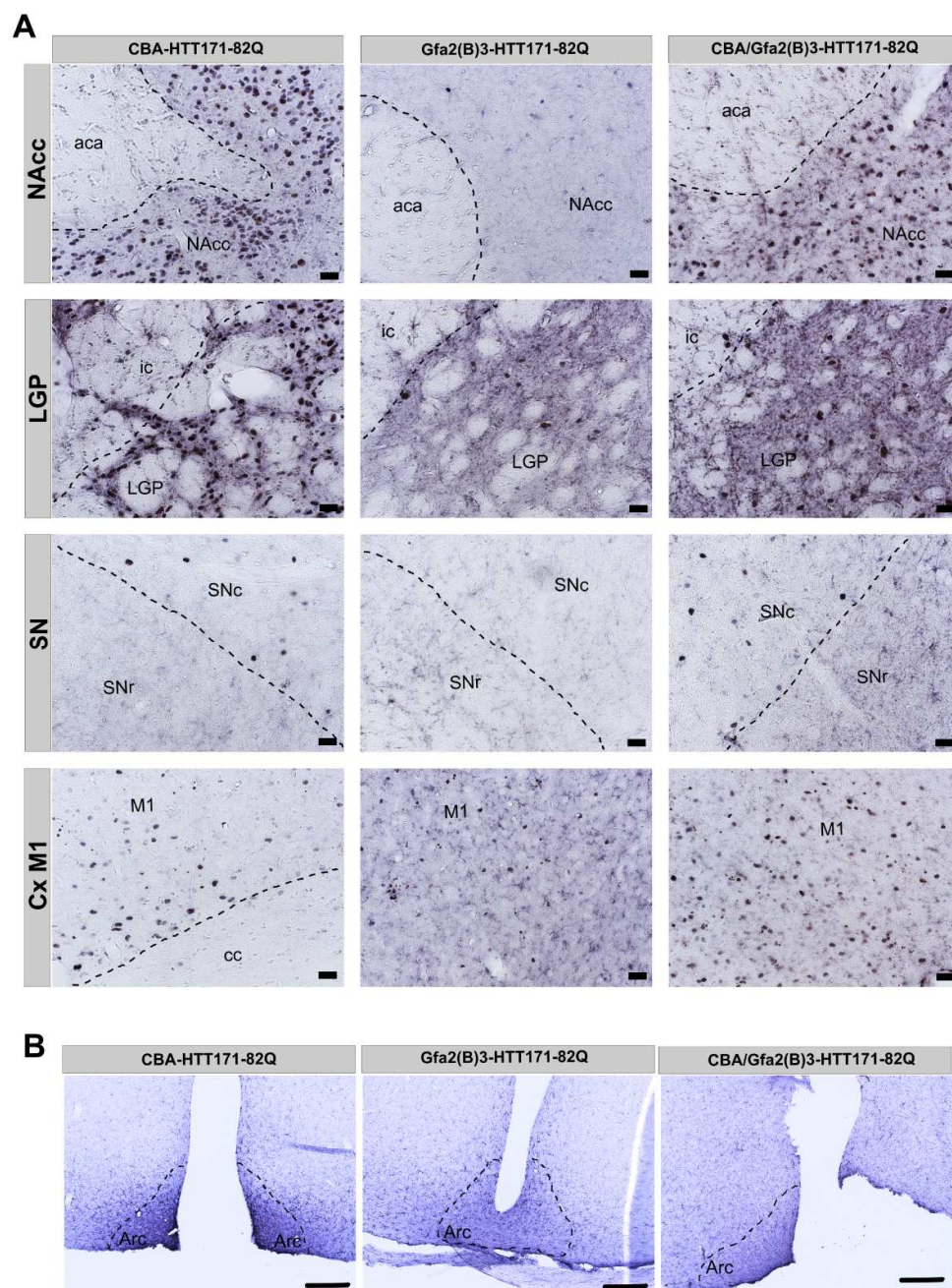
Figure S2: Characterization of mHTT aggregates in the striatum of the three mouse models.

(A) Representative pictures of striatal sections immunolabeled against aggregated HTT (EM48 antibody), for control mice injected with CBA-HTT171-18Q (left panel), Gfa2(B)3-HTT171-18Q (middle panel) or CBA/Gfa2(B)3-HTT171-18Q AAV2/5 (right panel) at 16 weeks post-injection. Scale bar = 20µm.

(B) Confocal acquisitions of eGFP, mHTT aggregates (Sicgen antibody) and either neuronal (NeuN) or astrocytic (GFAP) markers, that illustrate the absence of inter-cellular spreading of mHTT-positive aggregates 16 weeks after injection of either CBA-HTT171-82Q (upper panels) or Gfa2(B)3-HTT171-82Q (lower panels) viral vectors. Scale bar = 10µm.

Figure S3: Characterization of mHTT aggregates in part of the basal ganglia circuit of the three mouse models.
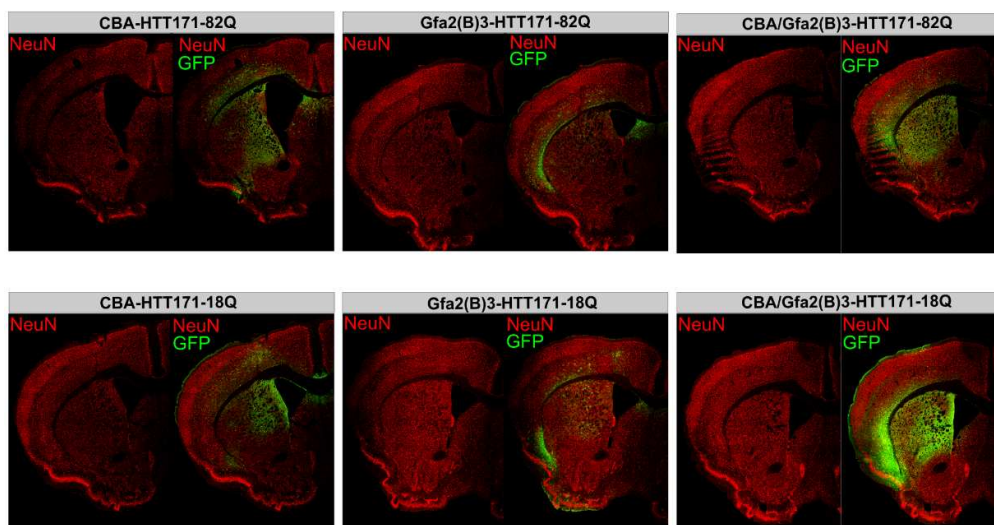

(A) Pictures of distinct basal ganglia structures stained for EM48 in CBA-HTT171-82Q (left panels), Gfa2(B)3-HTT171-82Q (middle panels) or CBA/Gfa2(B)3-HTT171-82Q (right panels) mice. Main structures are delimited by black dotted lines. NAcc = nucleus accumbens, LGP = lateral globus pallidus, SNc = substantia nigra pars compacta, SNr = substantia nigra pars reticulate, Cx M1 = primary motor cortex, aca = anterior commissure, anterior part, ic = internal capsule, cc = corpus callosum. Scale bar = 20μm.

(B) Low magnification pictures of the arcuate nucleus of the hypothalamus stained for EM48 16 weeks post-injection in CBA-HTT171-82Q mice (left panel), Gfa2(B)3-HTT171-82Q mice (middle panel) or
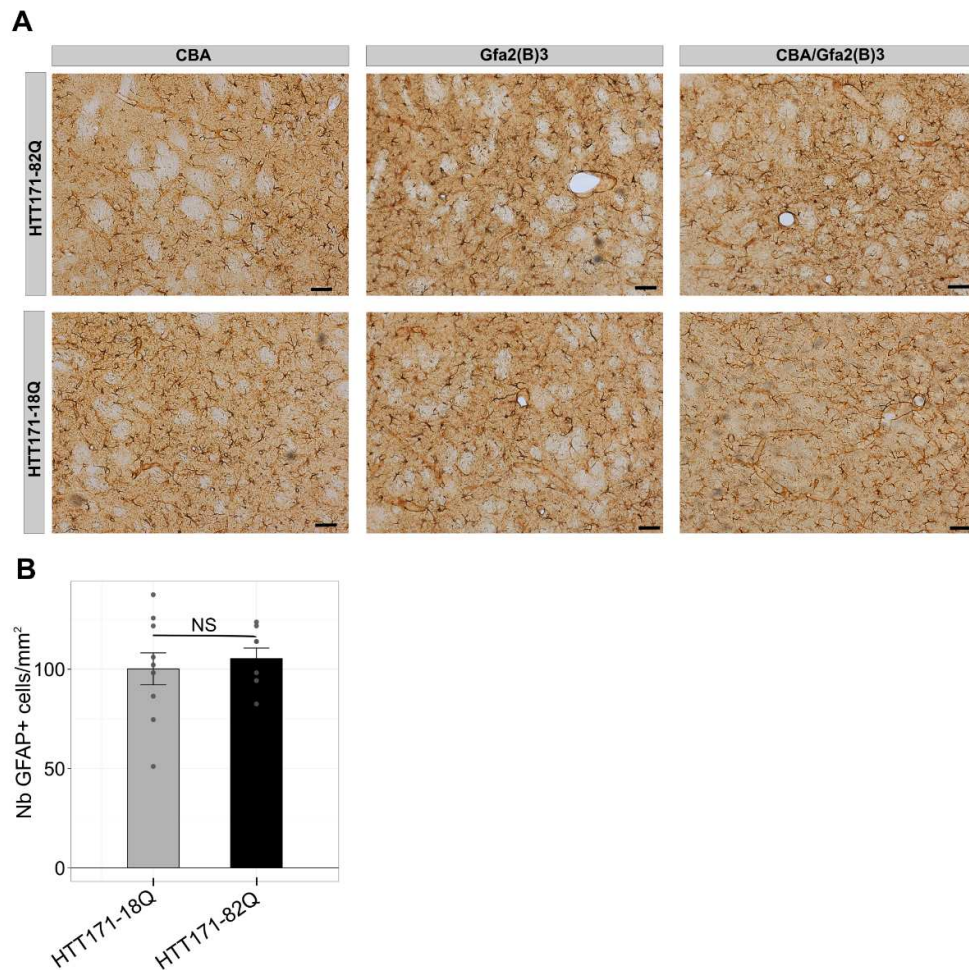
CBA/Gfa2(B)3-HTT171-82Q mice (right panel). Arc = arcuate nucleus of the hypothalamus. Scale bar = 200μm.

Figure S4: Evaluation of neuronal death in the three mouse models

Confocal mosaic acquisitions of sections immunolabeled for NeuN (left pictures) and GFP (right pictures) 16 weeks after injection in CBA-HTT171 mice (left panels), Gfa2(B)3-HTT171 mice (middle panels) or CBA/Gfa2(B)3-HTT171 mice (right panels). Mice expressing mutant HTT (82Q) are presented in upper panels. Mice with control HTT (18Q) are presented in lower panels. Co-immunolabeling with eGFP staining was performed to help the visualization of the injection area.

Figure S5: Characterization of the astrogliosis at 4 and 16 weeks post-injection.

A

B

(A) Low magnification pictures of Gfap immunolabelings of the mouse striatum 4 weeks after injection of AAV2/5 expressing CBA-HTT171 (left panels), Gfa2(B)3-HTT171 (middle panels) or CBA/Gfa2(B)3-HTT171 (right panels) with mutant (82Q, up panels) or control (18Q, low panels) *HTT*. Scale bar = 50μm.

(B) Quantification of the total number of Gfap-positive cells per mm^2 in the mice striatum 16 weeks after injection of CBA/Gfa2(B)3-HTT171-82Q (black bar) or CBA/Gfa2(B)3-HTT171-18Q (gray bar) viral vectors. Analysis was performed on 2 pictures/slice, 3 slices/n, n=8-10/group). Data represent mean ± SEM. Student's t test, NS: p. value ≥ 0.05.